Lithos 372–373 (2020) 105691

Contents lists available at ScienceDirect

Lithos

journal homepage: www.elsevier.com/locate/lithos

Research Article

Petrogenesis, platinum-group element geochemistry and geodynamic evolution of the Cretaceous Chilas gabbros, Kohistan island arc, NE Pakistan

Tehseen Zafar [a,g,*], Cheng-Biao Leng [a,b,*], Munazzam Ali Mahar [c], Masroor Alam [d,e], Xing-Chun Zhang [a], Wei Terry Chen [a], Hafiz Ur Rehman [f], Saif Ur Rehman [g]

[a] State Key Laboratory of Ore Deposit Geochemistry, Institute of Geochemistry, Chinese Academy of Sciences, Guiyang 550081, PR China
[b] State Key Laboratory of Nuclear Resources and Environment, East China University of Technology, Nanchang 330013, PR China
[c] Department of Geological Sciences, University of Texas at El Paso, El Paso, TX 79968, United States
[d] Department of Earth Sciences, Karakoram International University, Gilgit 15100, Pakistan
[e] China University of Geosciences, Beijing 100083, China
[f] Department of Earth and Environmental Sciences, Kagoshima University, Kagoshima 890-0065, Japan
[g] Institute of Geology, University of the Punjab, Lahore, 54590, Pakistan

ARTICLE INFO

Article history:
Received 30 November 2019
Received in revised form 14 July 2020
Accepted 15 July 2020
Available online 18 July 2020

Keywords:
Petrogenesis
Platinum-group element geochemistry
Tectonic evolution
Cretaceous Chilas gabbros
Kohistan arc

ABSTRACT

Kohistan, an intra-oceanic arc, formed due to the India-Asia collision-related tectonics. The arc is comprised of mafic-ultramafic and crustal lithologies. Chilas Complex, one of the major mafic-ultramafic body that lies at the base of the Kohistan arc, is dominantly composed of massive gabbronorites with local ultramafic-mafic intrusive bodies. The ultramafic rocks were considered as the products of fractional crystallization whereas gabbronorites were reported to have formed at the root zone of the magma chamber either from melts or due to fractional crystallization, based on major and trace element data. To understand the petrogenesis and origin of the Chilas gabbros, we conducted platinum group elements (PGEs) geochemistry combined with whole-rock major and trace element compositions. Geochemical data of the Chilas gabbros show tholeiite series, likely derived from a depleted lithospheric mantle source via peridotite melts. Presence of hornblende and relatively higher Al/Ti ratios of clinopyroxene in the Chilas gabbros suggest hydrous magma, ascribed to mantle wedge metasomatism by slab-derived fluids. Poor correlations between MgO vs. Ni, Cr, and V, Ni vs. Cr, Dy/Yb vs. SiO_2, Sr/Y vs. Eu/Eu* and relatively low TiO_2 indicate a minimal role of fractional crystallization. Low contents of LOI (0–3.24 wt%), Ce/Ce* (0.92–1.01), and positive relation of La, Ta, and Hf with Zr strongly support the insignificant impact of hydrothermal alteration. Enrichment of PGEs, such as Pt (0.63–13.75 ppb), Pd (0.43–13.87 ppb), and lower Pd/Ir ratios (0.76–40.04) suggest low degree partial melting of the parent magma. Higher Pd, Pd/Ir ratios compared to Pt and Pt/Pd, combined with enrichment of PPGE over IPGE, suggest the participation of slab-dehydrated fluids and mantle metasomatism however Cu/Ir vs. Ni/Pd, V-Pd/Ir and La-Pd/Ir ratios point towards olivine fractionation in the magma. Lower Cu/Pd ratios, relationships of Ru and Pt against Cr, and Os diminution corroborate S-undersaturation in parental magma. The PGEs contents and Pd/Pt ratios attest depleted mantle source for their production. In view of Cu/Zr and Cu/Pd ratios, it is substantiated that the sulphide segregation cannot be a promising reason for PGEs depletion. Therefore, we infer PGEs depletions in parental magma are due to PGEs-depleted mantle source, though sulfide retention in mantle source cannot be eliminated. The geochemical fingerprints in tectonic diagrams and negative anomalies of Nb and Zr in the studied samples provide credible facts that favour arc magmatism. Based on major and trace element data and PGEs values, we consider that the Chilas gabbros were formed from a lithospheric mantle that was metasomatized by fluids generated at the mantle wedge and derived from mafic melts in an arc setting. Geochemical data and their plotting on various tectonic discrimination diagrams indicate Chilas Complex as a remnant of the Neo-Tethyan oceanic arc system.

* Corresponding authors.
E-mail addresses: zafar@vip.gyig.ac.cn (T. Zafar), lcb8207@163.com (C.-B. Leng).

https://doi.org/10.1016/j.lithos.2020.105691
0024-4937/

1. Introduction

The Kohistan Island Arc (KIA), developed on account of northward subduction of the Neo-Tethys lithosphere under the Asian plate, is situated in northwest Himalaya, Pakistan (Fig. 1). The Cretaceous–Paleogene KIA is detached by two major suture zones, by the Main Karakoram Thrust in the north from the Asian plate, and by the Main Mantle Thrust in the south from the Indian plate (Fig. 1). Lithologically, the KIA can be classified into six major lithologic groups as (1) the Jijal and Sapat mafic-ultramafic complex that lies at the bottom of the arc, followed by (2) the Kamila Amphibolite, (3) Chilas Complex, (4) Kohistan Batholith, (5) metasedimentary, and (6) volcano-sedimentary series at the top (Fig. 1). Accordingly, Kohistan is one of the few places worldwide where a complete and exquisite arc structure from the oceanic upper mantle to the uppermost volcano-sedimentary series is conserved. Numerous studies have been conducted on geology, geochemistry, structure, and tectonics of the KIA (Khan et al., 1989; Burg et al., 1998; Jagoutz et al., 2006, 2007; Takahashi et al., 2007; Khan et al., 2009; Rehman et al., 2011 and references therein). Several authors proposed that KIA formed as a result of the northward subduction of the Neo-Tethyan oceanic lithosphere beneath the Asian Plate during Jurassic to Cretaceous times that further evolved through Paleogene. The ophiolites at the bottom of the KIA and volcanosedimentary sequences at the top suggest that the arc formed as a result of subduction and obduction of an oceanic lithosphere that evolved through multistage processes starting with the 110 and 95 Ma intrusive plutons of tonalites and diorites intrusive into the 120 to 99 Ma volcanosedimentary series at the top of the arc (Pudsey, 1986), the 117 to 95 Ma protolith age of the Jijal mafic-ultramafic complex at the bottom of the arc (Dhuime et al., 2007), the ~80 Ma amphibolite facies metamorphism of the Kamila (Khan et al., 1993) and the ~85 Ma formation age of the Chilas Complex as the root of the arc (Jagoutz et al., 2006, 2007), and the 102 to 26 Ma of the Kohistan Batholith in the middle (George et al., 1993). Khan et al. (1989) reported two dominant lithological varieties from the Chilas Complex, a massive (uniform) gabbro-norite association that roughly forms the 85% of the complex and a more diverse layered ultramafic-mafic-anorthosite association representing the rest of 15%. Based on structural appearance and xenoliths of gabbro-norites in ultramafic, the above authors interpreted the latter intruded into the former association. Moreover, the above authors concluded, based on whole-rock major and trace element data and mineral chemistry, that the ultramafic-mafic associations of the Chilas Complex represent cumulates of the gabbro-norites but intrusive features and some of the rare-earth element signatures (for details see Khan et al., 1989) were interpreted for melting of the sub-arc mantle source that was likely formed in a subduction-related island-arc environment. More recently, Bilqees et al. (2016), favoured the cumulate origin for the ultramafic-mafic association, based on the coexistence of olivine and orthopyroxene and highly calcic plagioclase but the origin of the massive gabbro-norite association was interpreted to be either a product of partial melting of a rising mantle diapir, cumulate, metasomatized and remobilized upper mantle. Contrary to that Kubo et al. (1996), based on field observations and geochemical dissimilarities argued for the cumulate origin and reported that ultramafic-mafic association is older than the gabbronorite. Jagoutz et al. (2007) also interpreted, based on major and trace element data, that the two associations are chemically distinct but likely derived from a common magma source due to the fractional crystallization process. To understand the origin and petrogenetic source of the dominant gabbro-norite association of the Chilas Complex, we analyzed major and trace element compositions of the whole rock samples along with platinum group elements geochemistry. So far, no studies have been conducted regarding metallogeny such as platinum group elements (PGEs) mineralization in connection to their tectonic settings. In this study, we investigated gabbroic rocks of the Chilas Complex for detailed field, petrological, and geochemical observations for the aims: (1) to understand petrogenetic and geodynamical evolution of Chilas gabbros based on major, minor and trace element compositions, (2) the role of trace, particularly rare-earth elements, on the fractionation of the parental magma, and (3) the importance of PGEs compositions on the melting aspects of the mantle source. The attained new geochemical data and interpretations, together with a new tectonic model, provide significant insights into the petrogenetic, PGEs, and tectonic development of the Chilas Complex.

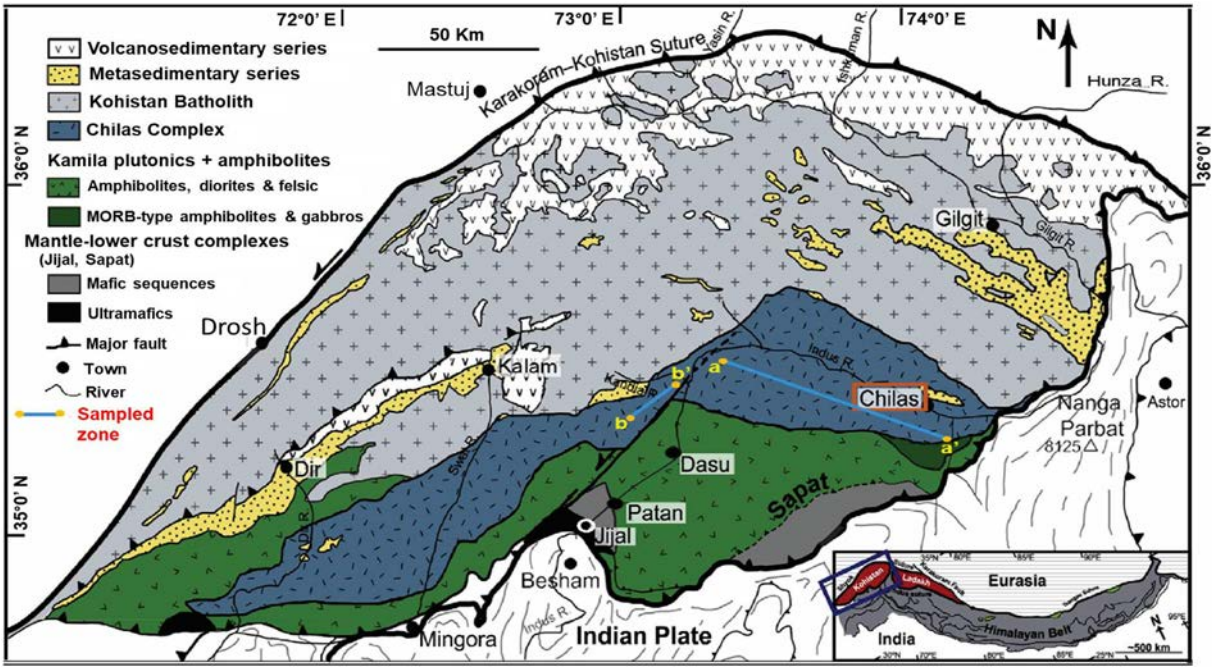

Fig. 1. Simplified geological map of the Kohistan island arc with its main lithotectonic units. The gabbro samples investigated in this study (collected along the two thick lines marked a-a' and b-b') were from the Chilas Complex. Map modified after Jagoutz (2014).

2. Geology of the Chilas Complex and sample description

The Chilas Complex is a gigantic mafic-ultramafic intrusion with the dimensions of 40 × 300 km and deduced as a magma chamber root zone of the KIA (Khan et al., 1989). It is mainly comprised of mafic (gabbronorites) lithologies (85%) and minor ultramafic rocks (15%), named as the ultramafic-mafic-anorthosite (UMA) association (Fig. 1). The UMA consists of numerous masses of pyroxenite, dunite, peridotite, gabbronorite, and anorthosite. Apart from these rocks, the Chilas Complex also contains several small bodies of diorites (Jagoutz et al., 2006). Pressure and temperature estimates show that these rocks were formed under conditions of 0.6–0.8 GPa and 600–800 °C (Bard, 1983). Originally, this complex has been deduced as a remnant of cumulate series of an oceanic crust or interpreted as a layered intrusion at the island arc base, that formed by mantle diapir (Khan et al., 1989). In contrast, the UMA dunites have been inferred as contact and reaction products of host peridotites and penetrating melts (Burg et al., 1998). Accordingly, the UMA units have been understood as apices of intra-arc mantle diapirs encroaching into the spreading island arc (Burg et al., 1998). Jagoutz et al. (2006) opined the ultramafic rocks as the surface expression of a vertically continuous upper mantle melt extraction system by which the basic series of the Chilas Complex was nourished. The gabbroic bodies of the Chilas intrude into amphibolite and contain several xenoliths of amphibolites that relate to the Kamila Amphibolites (Takahashi et al., 2007). The zircon U–Pb dating of the gabbros exposed in the Swat Valley yielded an age of 85–84 Ma (Schaltegger et al., 2002). In contrast, Ali et al. (2002), based on Sm–Nd isochron ages of gabbroic granulite, proposed older than 100 Ma magmatic ages for the Chilas Complex. Meanwhile, the cooling age of gabbroic rocks, based on K–Ar and ^{40}Ar–^{39}Ar methods, indicated 80 Ma (Treloar et al., 1990).

Best exposures of the UMA association are located typically in the eastern part of the Chilas Complex (Fig. 1). Samples of gabbroic rocks were collected from the Chilas Complex between longitudes 73°43′ 10.03″ to 74°02′11.95″ East and latitudes 35° 19′20.3″ to 35°31′46.48" North) (see Fig. 1 for sample location). The majority of the samples were fresh, massive, melanocratic to mesocratic, and characterized by medium- to coarse-grained textures. At outcrop-scale, augmentation of copper-bearing minerals (principally malachite and azurite) is obvious in the oxidized zones (Fig. 2a). Both the gabbroic bodies and ultramafic rocks depict interfingering, suggesting mutual or coeval intrusion of both varieties. Locally, disintegrated and deformed ultramafic xenoliths in gabbros (Fig. 2b) likely represent magma dynamics or assimilation. The xenoliths are darker and finer than the host gabbronorite and display irregular and diffused contact relations (Fig. 2b). Within the sequence of gabbroic rocks of Chilas, late-stage patchy as well as irregular hornblende-bearing pegmatites are frequently observed (Fig. 2c).

In total, 22 rock samples, collected from mafic associations of the Chilas Complex were investigated for petrography and geochemistry. Petrographically, the studied gabbros comprise olivine, clinopyroxene, and plagioclase, with minor constituents such as biotite, magnetite, amphibole, ilmenite, and chromite (Fig. 2d–f). The rocks are medium- to coarse-grained and display equigranular texture (Fig. 2d–f). Modal mineralogical composition of gabbroic rocks reveals ~12–16% olivine, ~27–34% pyroxene, ~46–52% plagioclase, and ~3–5% accessory phases of amphibole, biotite, and opaque minerals such as ilmenite and magnetite. Based on corresponding textural characteristics, gabbros exhibit predominantly accumulate nature and occasionally indicate granoblastic texture at a number of places. Petrographic observations show the original magmatic textures are still preserved in these gabbros indicating the rocks did not undergo variable degrees of hydrothermal alteration (Fig. 2d–f).

Observation of the gabbroic bodies under ore microscopy and scanning electron microscope (SEM) reveals the presence of sulphide mineralization, principally chalcopyrite (ccp), pyrrhotite (po), pentlandite (pn), pyrite (py), galena (gn), laurite, and platinum group minerals such as irarsite (Irs) (Fig. 2g–l). Normally, sulphides occur in an irregular, disseminated form and also observed in the form of stringers at places (Fig. 2g–l). The predominant sulphide mineralization associated with gabbros such as chalcopyrite, pyrrhotite, pyrite, and pentlandite seems to be primary. Pyrrhotite is normally developed at the edges of chalcopyrite.

3. Analytical methods

Relatively fresh and less weathered representative samples (n = 22) of gabbroic rocks were selected for petrographic and geochemical analysis. The petrographic study of the prepared slides was conducted by polarizing and ore microscopy. The sulphides and PGM were analyzed using back-scattered electron (BSE) imaging at the State Key Laboratory of Ore Deposit Geochemistry (SKLODG), Institute of Geochemistry, Chinese Academy of Sciences, Guiyang. BSE imaging was performed using a JSM-7800 thermal field emission Scanning Electron Microscope (FE-SEM) connected with Energy Dispersive Spectrometer (EDS). Polished blocks were examined analytically for sulphides and PGM by four quadrants back scattered electron detector at the magnification of ×500. Finally, images were photographed through 4 quadrants back-scattered detector operating at 20 kV accelerating voltage, a beam current of 20 Na, 1000 ms/step counting time, and a working distance of 10 mm.

The selected 22 samples were washed by distilled water, and then rock powder was prepared into glass discs by fusion with lithium metaborate for whole-rock analysis. The representative powders of gabbroic rocks were nominated for major and trace elemental evaluation. Major and minor oxides of the gabbros were determined by X-ray fluorescence (XRF) whereas, trace elements including rare earth elements (REEs) were examined by Inductively-Coupled Plasma Mass Spectrometer (ICP-MS) and the results are shown in Tables 1 and 2. The analytical protocol was the same as presented elsewhere (Qi et al., 2000). The analytical precision for measured elements is better than 5%.

Contents of PGEs were measured, from a sample powder weighing about eight grams, by isotope dilution ICP-MS (ID-ICP-MS) using the Carius tube scheme and the results are shown in Table 3. Contents of Rh were measured by ^{194}Pt as the internal standard however, concentrations of other PGEs including Ru, Pd, Pt, and Ir were determined through ID-ICP-MS. The geochemical standard was WGB-1 to check the quality of the instrument. The overall procedural blanks were less than 0.003 ppb for Ru and Ir; 0.012 ppb for Pd and 0.002 ppb for Pt and Rh, respectively. For all PGEs, the analytical accuracies are assessed to be better than 20%.

4. Results

4.1. Bulk-rock major and trace elements

Major and trace element compositions of gabbros from the Chilas Complex exhibit a narrow range of SiO_2 (42.56–54.60 wt%), moderate range of CaO (6.12–14.99 wt%), low MgO (4.16–7.75 wt%), K_2O (0.06–0.99 wt%), Na_2O (1.27–4.62 wt%), P_2O_5 (0–0.58 wt%) and TiO_2 (0.22–1.66 wt%). Al_2O_3 indicates moderate concentrations ranging from 12.37–19.93 wt% and Fe_2O_3 reveals higher contents ranging between 5.03 and 15.02 wt%. The total alkali-silica (TAS) diagram displays the majority of the rocks as gabbro (Fig. 3a) with geochemical traits of metaluminous and tholeiitic character (Fig. 3b–d). The samples show variable values of loss on ignition (LOI) between 0.0 and 3.24 wt%. The Chilas gabbros are characterized by variable contents of compatible trace elements including Cr (173–369 ppm), Ni (24.73–150.01 ppm), and Co (25.52–46.30 ppm). Incompatible large ion lithophile elements (LILEs) denote fairly significant amounts (Sr = 217–497 ppm, Ba = 53.90–264 ppm, Rb = 0.65–18.10 ppm). Further, high field strength elements (HFSEs) specifically Ta (0.095–0.475 ppm), Hf (0.70–4.72 ppm), Nb (1.65–6.46 ppm), U (0.02–1.08 ppm) and Th (0.03–2.64 ppm), display depleted amounts except for Zr that expresses comparatively

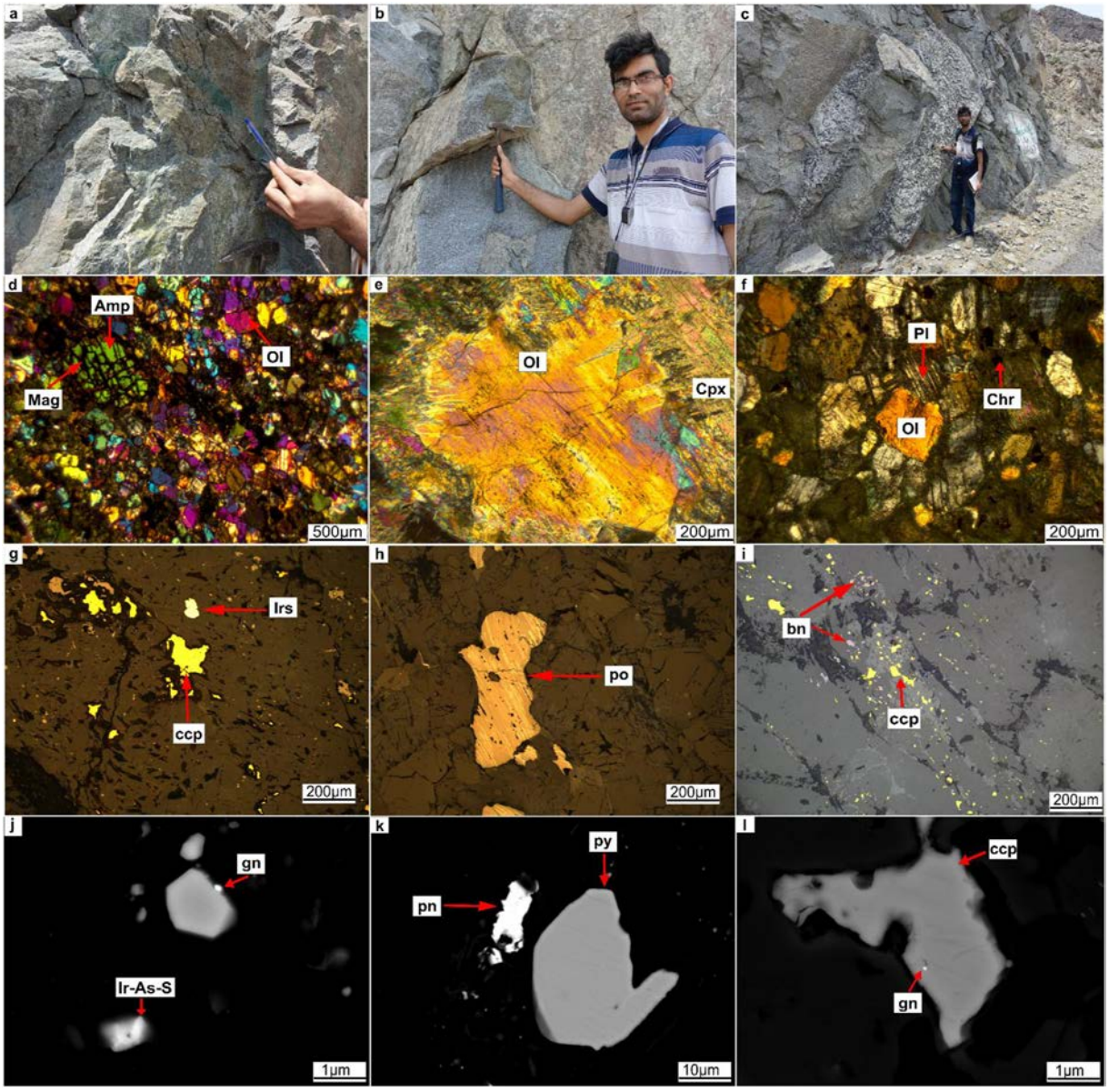

Fig. 2. Representative photographs of field outcrops, thin sections, and BSE images: (a) Copper mineralization in host Chilas gabbros; (b) Ultramafic xenoliths in gabbro; (c) Plagioclase (Pl) and amphibole (Amp) rich irregular pegmatitic dyke in gabbro; (d) Presence of olivine (Ol) and anhedral inclusion of magnetite (Mag) in amphibole; (e) Occurrence of fractured olivine crystal with clinopyroxene (Cpx); (f) Olivine (Ol) crystal enclosed by plagioclase laths. Chromite (Chr) grains are also present; (g-l) Occurrence of sulphide mineral assemblage and irarsite in gabbroic rocks. Abbreviations: bn = bornite; ccp = chalcopyrite; gn = galena; pn = pentlandite; po = pyrrhotite; py = pyrite; Irs (Ir-As-S) = irarsite.

greater ranges from 25.20 to 210 ppm. The primitive mantle-normalized and REE chondrite patterns are characterized by LILEs-LREEs enrichment over the depleted HFSEs and HREEs (Fig. 4a–b). These normalized patterns display pronounced negative anomalies of Zr, Nb, Th, and Rb (Fig. 4a). Moreover, the studied rocks show insignificant or weak correlations among various elements (e.g. MgO with Cr and Ni, Cr with Ni and V, Fig. 6b–e). Contrarily, in the bivariate plots, trace elements like Ta, Hf, La, Y, and Rb express positive relations with Zr (Fig. 8b–f).

4.2. Bulk-rock PGEs geochemistry

The analyses (Table 3) show low contents of PGEs in the studied samples (i.e., Ir: 0.14–0.69 ppb, Ru: 0.57–1.69 ppb, Rh: 0.06–1.59 ppb, Pd: 0.43–13.87 ppb, and Pt: 0.63–13.75 ppb). The Pd/Ir and Cu/Pd ratios range from 0.76 to 40.04 (with a few exceptions of 77.05, 85.93, and 11.55 to 3161.29, respectively).

The results indicate the depletion of the Iridium Group (IPGEs) compared with the Palladium Group (PPGEs) (Table 3). Copper (Cu) is fairly augmented in several samples of the studied rocks however they are deficient in MgO (Table 2). Though the total content of PGEs is low in Chilas gabbros, prominent and progressive enhancement of Pd over Pt has been noticed (Table 3). The studied samples have Pd/Pt (0.12–1.31) and Pd/Ir (0.76–40.04, exception of 77.05 and 85.93 in two samples) ratios higher in comparison to primitive mantle (Pd/Pt = 0.53; Pd/Ir = 1.01). In contrast, the Pt/Pd ratios exhibit a range of 0.76–7.89. The studied samples indicate strong fractionated PGEs (Pd/Ir ≈ 0.76–40.04, exception of 77.05, 85.93). The bivariate plots indicate olivine governance on the distribution of PGEs (Fig. 9a–c), while plots of Ru and Pt against Cr show S-undersaturation and fractionation (Fig. 9e–f).

Table 1
Major elements (wt%) of the gabbroic rocks from the Chilas Complex.

Samples	SiO_2	Al_2O_3	Fe_2O_3	MgO	CaO	Na_2O	K_2O	MnO	P_2O_5	TiO_2	LOI	Total
S3-B	53.70	16.92	8.63	5.99	8.47	3.24	0.62	0.132	0.104	0.598	0.99	99.39
S5-B	53.18	16.53	9.49	5.03	8.59	3.55	0.62	0.156	0.318	1.303	1.83	100.60
S6-A	47.98	17.08	12.77	6.06	6.12	2.68	0.84	0.146	0.171	0.847	3.24	97.93
S6-C	52.15	17.74	10.30	5.15	6.79	3.15	0.96	0.139	0.282	0.772	2.19	99.63
S8-B	54.60	17.02	8.79	4.77	7.94	3.21	0.71	0.139	0.293	0.906	1.59	99.97
S8-B-2	54.47	17.00	8.76	4.76	7.91	3.17	0.72	0.141	0.289	0.901	1.61	99.73
S9-B	52.02	17.32	8.72	4.77	8.88	3.39	0.97	0.136	0.163	0.837	2.17	99.37
S10-A	54.28	16.89	9.63	5.17	8.26	3.33	0.86	0.149	0.197	0.786	0.17	99.72
S11-A	51.22	18.25	9.35	4.96	8.95	3.28	0.27	0.138	0.236	1.064	1.97	99.69
S11-B-1	51.60	17.47	9.16	5.05	8.99	4.62	0.46	0.140	0.247	1.031	0.78	99.55
S16-A	42.56	12.37	10.21	7.65	14.99	1.27	0.41	0.143	0.588	1.669	1.59	93.45
S16-D	54.57	16.69	7.94	4.16	8.97	3.62	0.99	0.116	0.185	0.769	0.66	98.67
S20-A	45.38	16.37	15.02	7.75	9.73	2.70	0.41	0.238	0.080	1.044	1.13	99.86
S20-B	47.24	19.09	11.10	6.10	10.03	3.17	0.35	0.184	0.127	0.867	1.07	99.32
S-21	52.79	16.97	10.42	5.54	9.33	2.77	0.30	0.162	0.214	0.883	0.00	99.38
S24-A	54.01	17.19	9.56	4.21	8.36	3.10	0.79	0.149	0.223	1.050	1.68	100.32
S25-C	49.55	19.76	8.58	4.46	9.88	3.20	0.98	0.143	0.205	0.650	1.00	98.41
S25-D	49.17	18.34	10.53	4.58	9.94	3.29	0.82	0.154	0.297	1.551	0.20	98.87
S33-B	52.67	19.72	7.91	4.65	8.70	3.87	0.21	0.120	0.140	0.677	0.83	99.50
S-36	49.85	19.93	5.03	6.49	11.89	2.74	0.06	0.137	0.000	0.220	2.05	98.39
S-37	50.53	17.25	11.56	5.18	11.52	2.21	0.14	0.172	0.272	1.130	0.25	100.21
S-39	50.48	19.36	10.78	6.15	8.94	2.69	0.12	0.166	0.141	0.950	0.15	99.92

5. Discussion

5.1. Petrogenetic aspects

5.1.1. Nature of the magma source

The studied gabbroic rocks indicate subduction-like geochemical attributes, are slightly augmented in LREEs, LILEs, and are deficient in HFSEs specifically Nb, Ti, and Zr (Fig. 4a; Table 2). HFSEs (for example Ta, Zr, Nb, Ti), as well as HREEs, are considered as immobile during convergence (Xu et al., 2003). The Zr to Nb ratio can conceivably reveal mantle enrichment or depletion (Geng et al., 2011) and data from the Chilas gabbros plot in the field of the depleted mantle (Fig. 5a). This is further supported by the δNb values ($\delta Nb = 1.74 + \log(Nb/Y) - 1.92\log(Zr/Y)$) of representative samples exhibiting a range from −0.69 to 0.57 where the negative values can reflect also a depleted mantle source. In general, Nb/Th and Zr/Nb can be significant to define the nature and source characteristics of the mantle. For instance, most of the studied gabbro samples exhibit Nb/Th < 8 except for a few samples and higher Zr/Nb ratios (12.87–35.07), again imply their source derivation from a depleted mantle (Condie, 2015). It is reported that gabbroic bodies produced from asthenospheric mantle generally have La/Nb ratios lower than 1.5 and La/Ta ratios <22 (Saunders et al., 1992). Contrarily, the Chilas gabbros have higher La/Nb (1.95–5.80) and La/Ta (27.17–63.03) ratios, demonstrate that their origin was from the lithospheric mantle. This interpretation is further supported by the Nb/La vs. La/Yb diagram which points towards the lithospheric mantle source (Fig. 5b).

It is widely accepted that the mantle source for mafic rocks is controlled by peridotite (Falloon et al., 2008). However, modern researches have reported that hornblendite, pyroxenite, and carbonated peridotite can also yield mafic rocks, particularly for Ocean-Island-Basalts (OIB) with intraplate basalt geochemical signatures (e.g., Brunelli et al., 2018). The ratios of Zn/Fe are typically distinct in pyroxenite and peridotite, therefore it can be important to discriminate the lithology of mantle source. The geochemical data (Ni vs. MgO and Zn/Fe ratios) of studied samples fall in the domain of peridotite melts and their evolutional melt curves (Fig. 5c). Compared with the experimental melt compositions, the measured primary melts of the rock samples express affinity with volatile-free peridotite (Fig. 5d). Collectively, all these confirmations, together with the tholeiitic nature, propose that the mantle source of the mafic magmatism in Chilas Complex is ruled by peridotite.

REEs ratios are extensively used to define the origin of the spinel or garnet-bearing magmas that form gabbros (Xu et al., 2005). For example, Dy/Yb vs. La/Yb ratio can be a valuable tool to restrain the source mineralogy of gabbros. The gabbros display lower Dy/Yb (1.61–1.90), Sm/Yb (1.34–1.99), and La/Sm (1.45–4.63) ratios, and all the samples fall close to the field of spinel peridotite on the Dy/Yb vs. La/Yb diagram (Fig. 5e), further represent that the magma source of the Chilas gabbros was spinel-bearing mantle peridotite. The relatively lower Sm/Yb (1.34–1.99) and Gd/Yb (1.53–1.98) ratios in the Chilas gabbros suggest that their primary magmas were derived from a shallow mantle source. Moreover, low Ce/Y ratios (0.54–1.85, i.e. <2) of the Chilas gabbros further point to a magma generated in the spinel stability field at a depth of about 60–80 km (McKenzie and Bickle, 1988).

On the spider diagram of Chilas rocks (Fig. 4a), the noticeable LREEs and LILEs enrichment and obvious depletion of Ti and HFSEs portray geochemical signatures of subduction-related magmatism, signifying that subducted material may have incorporated into the mantle source. On the La/Nb vs. Nb/Th plot, the studied samples fall in an arc gabbro field (Fig. 5f).

5.1.2. Composition of the magma

Gabbroic rocks can form from a dry or wet basaltic magma through a process of fractional crystallization (Gaetani and Grove, 1998). The existence of subhedral to anhedral amphibole in the Chilas gabbros (Fig. 2f) indicates its primary igneous texture and suggests its crystallization directly from a magma that was somewhat hydrous.

Moreover, the chemical composition of clinopyroxene also significantly points to the water content of a magma. In dry mafic magmas (such as tholeiitic and silica-undersaturated) clinopyroxene incorporates Al in the $CaTiAl_2O_6$ molecule via coupled substitution of $^{vi}Mg^{iv}Si_2$ to $^{vi}Ti^{iv}Al_2$ (Loucks, 1990). This replacement is stimulated through high titanium activity relative to silica in the melt and therefore, considered as the main characteristic of silica-undersaturated dry basaltic source. In contrast, clinopyroxene, in hydrated magmas with greater fugacities of O_2 and H_2O, endorse replacement between $^{vi}Mg^{iv}Si$ and $^{vi}Fe^{3+}\ ^{iv}Al$, and consequently, Al incorporates in the $CaFe^{3+}AlSiO_6$ molecule (Loucks, 1990). Clinopyroxenes in the Chilas gabbros, having relatively higher Al/Ti ratios (data from Jagoutz et al., 2007), indicate hydrous magma that produced these gabbros. However, it is still a question to solve whether the magma hydrated in the crust or mantle. As

Table 2
Trace elements (ppm) compositions of the gabbros from the Chilas Complex.

Samples	Li	Be	Cr	Co	Ni	Cu	Zn	Rb	Sr	Y	Zr	Nb	Cs	Ba	La	Ce
S3-B	11.09	1.03	369	31.50	79.50	46.20	80.40	3.81	405	19.80	44.30	2.22	0.183	157	9.77	21.40
S5-B	12.30	0.96	275	26.41	46.23	111	76.00	5.14	422	19.83	109	5.31	0.341	175	10.40	23.41
S6-A	23.34	0.82	228	35.82	106.01	8140	134	9.60	335	15.80	75.81	3.40	0.842	210	11.30	23.50
S6-C	15.90	1.01	215	32.70	57.23	1290	108	10.50	364	15.13	40.20	2.87	1.150	177	13.30	28.00
S8-B	8.00	1.05	237	28.20	40.91	38.91	78.51	7.81	397	21.83	73.60	3.54	1.690	164	12.31	26.43
S8-B-2	6.95	0.84	188	29.93	46.83	95.00	70.00	2.99	400	18.30	45.81	2.97	0.262	121	8.47	19.20
S9-B	20.10	1.02	292	29.70	51.22	165	82.32	13.30	393	18.81	66.10	2.76	0.214	225	9.57	21.44
S10-A	10.60	0.95	273	31.62	49.73	230	86.51	11.20	382	23.10	94.70	2.70	0.208	197	10.60	24.11
S11-A	17.61	0.89	184	31.73	50.52	109	71.40	1.38	395	18.63	61.41	3.08	0.093	102	8.45	19.10
S11-B-1	7.07	0.86	183	30.23	46.70	95.80	69.92	3.02	401	18.31	48.01	3.03	0.268	122	8.49	19.21
S16-A	13.40	1.03	270	34.91	150.01	34,300	78.10	5.31	217	48.13	112	3.89	0.088	110	13.90	34.80
S16-D	14.32	1.07	236	26.70	87.53	7620	65.10	17.50	352	27.62	99.31	3.28	0.305	176	11.50	27.00
S20-A	16.53	0.77	243	46.30	62.91	187	128	1.66	317	31.50	35.80	2.78	0.059	53.90	6.13	17.23
S20-B	14.33	0.69	178	37.92	49.23	246	92.73	1.19	436	20.51	26.92	2.02	0.044	57.93	5.35	14.12
S-21	5.78	0.84	222	34.00	38.10	44.01	81.12	1.96	403	20.73	79.11	2.97	0.023	108	10.30	22.60
S24-A	22.23	1.07	174	27.84	24.73	41.10	73.74	10.50	398	23.85	90.30	4.98	0.041	215	13.70	29.11
S25-C	9.19	1.12	189	26.73	40.92	3820	79.42	10.30	497	16.52	38.70	2.24	0.188	230	13.00	26.40
S25-D	11.82	1.10	173	30.60	36.41	2500	82.43	18.10	488	20.61	210	6.46	0.373	264	12.91	26.91
S33-B	6.11	0.80	229	26.50	45.83	53.90	64.50	0.65	492	11.50	25.20	1.65	0.061	83.60	4.92	11.10
S-36	9.17	1.14	185	25.52	39.81	3830	78.53	10.20	493	15.70	36.81	2.28	0.185	226	13.20	25.81
S-37	14.82	1.04	211	32.51	55.72	1280	105	11.30	367	15.62	39.83	2.83	1.170	179	13.50	27.10
S-39	21.62	0.85	225	36.70	105.02	8135	136	9.40	336	15.53	75.60	3.44	0.863	215	11.71	23.80

Samples	Pr	Nd	Sm	Eu	Gd	Tb	Dy	Ho	Er	Tm	Yb	Lu	Hf	Ta	Th	U
S3-B	2.82	12.30	3.05	1.00	3.24	0.548	3.35	0.707	2.01	0.314	2.00	0.307	1.32	0.155	0.314	0.093
S5-B	3.14	13.71	3.33	1.13	3.50	0.575	3.39	0.709	1.98	0.294	1.85	0.285	2.75	0.360	0.605	0.222
S6-A	2.91	11.93	2.61	0.91	2.72	0.432	2.60	0.550	1.59	0.250	1.61	0.248	2.12	0.333	0.587	0.445
S6-C	3.43	13.90	2.87	1.02	2.90	0.435	2.49	0.528	1.50	0.233	1.52	0.242	1.14	0.232	0.854	0.202
S8-B	3.50	15.00	3.51	1.07	3.67	0.596	3.52	0.741	2.07	0.310	1.96	0.301	1.97	0.249	0.893	0.301
S8-B-2	2.62	11.81	2.97	1.07	3.17	0.525	3.11	0.655	1.83	0.275	1.74	0.264	1.33	0.203	0.530	0.230
S9-B	2.87	12.43	3.06	0.89	3.20	0.541	3.24	0.671	1.90	0.289	1.84	0.279	1.87	0.191	0.416	0.130
S10-A	3.25	14.40	3.64	1.05	3.86	0.651	3.91	0.828	2.34	0.356	2.27	0.351	2.43	0.189	0.750	0.224
S11-A	2.64	11.82	2.99	1.08	3.19	0.534	3.19	0.669	1.87	0.280	1.76	0.270	1.64	0.207	0.476	0.263
S11-B-1	2.62	11.80	2.96	1.07	3.17	0.523	3.10	0.658	1.82	0.272	1.73	0.264	1.36	0.207	0.536	0.232
S16-A	4.88	22.23	6.21	1.25	7.13	1.290	8.10	1.720	4.78	0.704	4.25	0.624	3.27	0.284	2.640	0.808
S16-D	3.75	16.91	4.46	1.14	4.74	0.803	4.82	1.000	2.77	0.411	2.58	0.384	2.74	0.236	0.916	1.080
S20-A	2.86	14.43	4.20	1.38	4.76	0.846	5.21	1.110	3.16	0.484	3.11	0.479	1.39	0.121	0.084	0.044
S20-B	2.12	9.90	2.74	1.10	3.11	0.547	3.41	0.732	2.06	0.316	2.03	0.312	1.02	0.096	0.054	0.026
S-21	3.00	13.00	3.21	1.02	3.46	0.576	3.48	0.731	2.09	0.315	1.99	0.308	2.09	0.214	0.993	0.244
S24-A	3.76	16.13	3.88	1.13	4.07	0.670	4.02	0.848	2.40	0.367	2.32	0.360	2.34	0.345	0.403	0.138
S25-C	3.30	13.71	3.07	1.07	3.04	0.474	2.75	0.576	1.61	0.247	1.57	0.244	1.27	0.215	1.300	0.234
S25-D	3.49	14.80	3.50	1.14	3.67	0.584	3.46	0.723	2.03	0.303	1.94	0.305	4.72	0.475	1.340	0.360
S33-B	1.54	7.00	1.81	0.78	1.92	0.322	1.97	0.415	1.17	0.179	1.15	0.175	0.70	0.095	0.030	0.021
S-36	3.27	13.81	3.09	1.06	3.07	0.485	2.77	0.573	1.63	0.249	1.55	0.246	1.25	0.217	1.330	0.237
S-37	3.47	14.72	2.92	1.05	2.93	0.447	2.51	0.523	1.53	0.235	1.54	0.244	1.17	0.242	0.867	0.205
S-39	2.93	11.70	2.65	0.91	2.75	0.437	2.65	0.565	1.62	0.260	1.63	0.245	2.15	0.335	0.595	0.448

Table 3
PGEs (ppb) compositions of the gabbros from the Chilas Complex.

Samples	Ir	Ru	Rh	Pt	Pd
S3-B	0.43	1.54	0.61	1.95	2.09
S5-B	0.24	0.57	0.84	8.45	9.61
S6-A	0.61	1.03	1.04	4.83	3.57
S6-C	0.18	1.17	1.59	10.55	13.87
S8-B	0.22	0.85	0.06	3.17	1.36
S8-B-2	0.55	0.89	0.09	0.63	0.61
S9-B	0.56	1.27	0.47	1.13	0.43
S10-A	0.41	1.49	0.64	1.91	2.03
S11-A	0.20	1.14	0.15	5.20	1.48
S11-B-1	0.59	0.86	0.08	0.65	0.64
S16-A	0.67	1.69	0.86	13.75	10.85
S16-D	0.69	1.13	1.06	6.57	3.43
S20-A	0.26	1.51	0.34	9.23	5.53
S20-B	0.23	1.34	0.32	4.19	1.59
S-21	0.14	1.29	0.65	3.67	0.62
S24-A	0.15	0.81	0.51	6.59	0.86
S25-C	0.57	0.87	1.29	10.40	9.53
S25-D	0.17	0.76	0.31	10.70	4.57
S33-B	0.14	0.86	0.54	6.63	0.84
S-36	0.63	0.79	0.56	5.19	3.07
S-37	0.16	1.33	1.58	13.65	13.75
S-39	0.28	1.55	0.37	8.21	5.59

stated above, the crystallization of hornblende necessitates the magma to have high-water content (>3 wt%; Sisson and Grove, 1993). In fact, experimental and direct analysis on natural rock samples indicates that both the lithospheric and asthenospheric mantle contain small amounts of water ca. <0.1 wt% (e.g., Williams and Hemley, 2001). However, mantle wedge can be generally metasomatized through the participation of subduction-derived fluids (e.g., McInnes et al., 2001) thus can retain higher amounts of water reaching up to 12 wt% (Gaetani and Grove, 1998). Considering these aspects, we assume that the parental magma to the Chilas gabbros became hydrated and enriched in consequence of mantle wedge metasomatism and input of slab-derived fluids.

5.1.3. Cumulates versus crystallized melts for the Chilas gabbros

Although field and petrographic study of Bilqees et al. (2016), favoured the cumulate origin for the ultramafic-mafic association of Chilas Complex based on cumulate textures and igneous layering, which may be plausible. However, the origin of the massive and dominant unit of the gabbro-norite association was vaguely interpreted. Various authors have favoured their origin as cumulates whereas others proposed their formation from mafic melts at the root zone of the

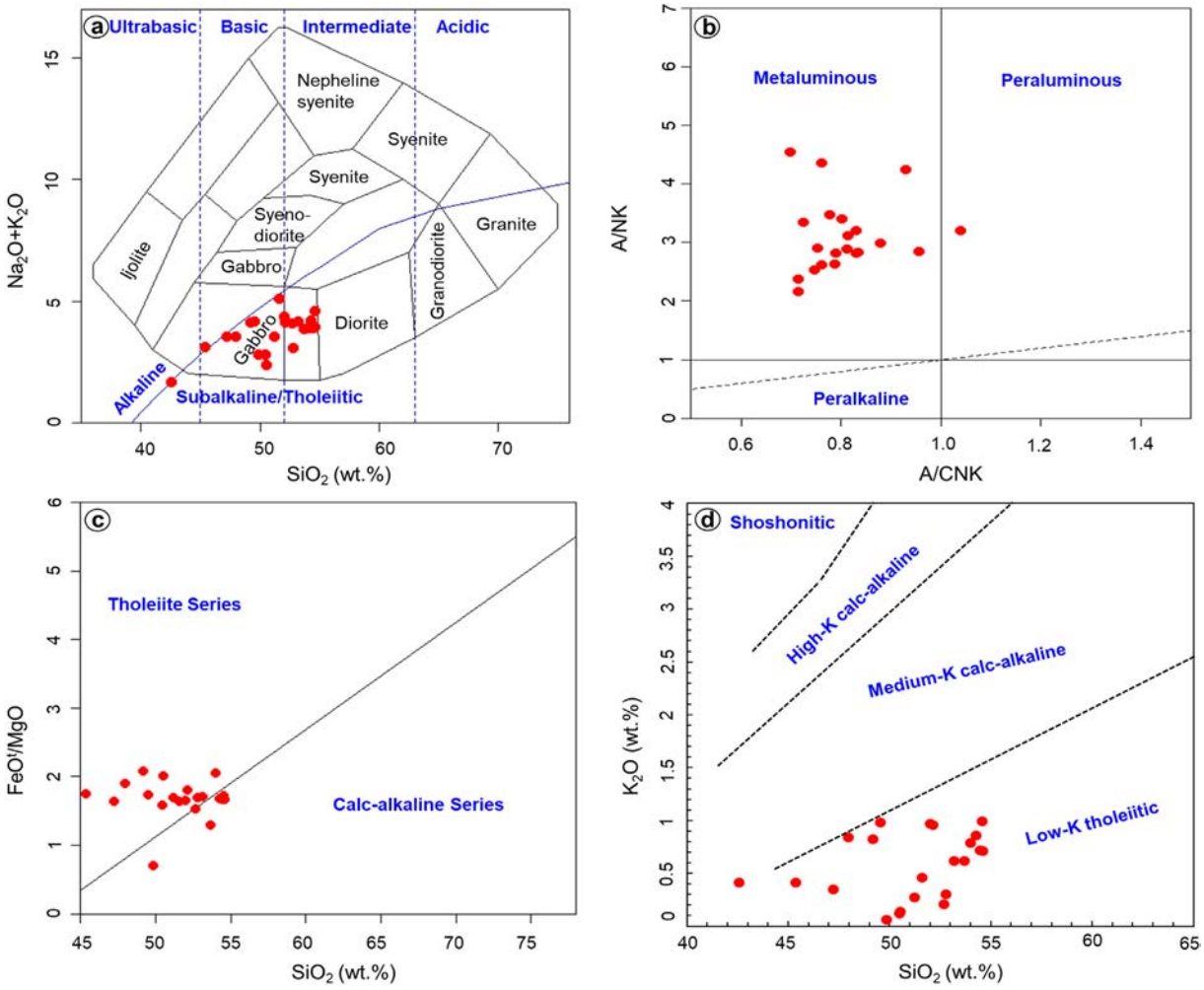

Fig. 3. Geochemical diagrams for the Chilas gabbro: (a) $Na_2O + K_2O$ vs. SiO_2 (Cox et al., 1979); (b) A/CNK vs. A/NK (Shand 1943); (c) FeO^T/MgO vs. SiO_2 (Miyashiro, 1974); and (d) K_2O vs. SiO_2 (Middlemost, 1985).

magma chamber in subduction settings. Our geochemical data favours non-commutate origin particularly for the massive gabbroic part, therefore our interpretation is most likely to the non-cumulate origin.

It is widely reported that the gabbroic rocks at convergent boundaries formed by crystal accumulation or crystallized from melts can be distinguished by their field features, textural characteristics, and geochemical signatures. Chilas Complex dominantly represents massive gabbros (Fig. 2a–f) with local layering. Chilas gabbros reveal mutually cross-cutting associations and syndepositional structures which might be due to seismic shaking, however slumping is most likely linked to the turbulence of magma (Bilqees et al., 2016). Local folding, slumping, and folding makes it hard to identify primary cumulate texture or different stages of crystallization from melts. However, geochemical data, particularly, immobile trace elements and REE, can play a significant role in identifying the process of their formation. The majority of the studied rock samples display negative Eu anomalies and elevated values of LREEs (Table 1; Fig. 4), effectively rule out plagioclase accumulation in their formation. The Chilas gabbros having low but variable MgO contents (Table 1) and preserving interstitial hornblende (Fig. 2d) demonstrate that amphibole accumulation was trivial. The noticed contents of REEs are not extremely low, thereby indicating another clue in favour of their non-cumulate origin. Apart from these facts, the studied samples of Chilas gabbros mainly plot in the field of arc-related mafic-non cumulate origin with some overlap for the cumulate field (Fig. 10b). It is not very clear if the Chilas gabbros are entire of cumulate origin but may have crystallized from melts, therefore reflect characteristics of primary basaltic magma. Based on some of the geochemical signatures, the Chilas gabbros can be comparable with the Gangdese gabbroic rocks of the southern Tibet that are also interpreted as of non-cumulate origin (Wang et al., 2019).

5.1.4. Role of fractional crystallization

The examined samples of Chilas Complex reveal low and slight variable MgO contents (4.16–7.75 wt%) which imply their derivation from primitive instead of evolved magmas, therefore, may not represent successive fractional crystallization. Likewise, the higher Fe_2O_3 (5.03–15.02 wt%) of these rocks reflect the primary chemistry of the magma that shows insignificant fractionation or differentiation during the magma ascent. The relatively low TiO_2 (0.22–1.66 wt%) and MgO (4.16–7.75 wt%) point out the minimal fractionation of plagioclase and Ti-bearing minerals during magmatic differentiation. More importantly, it is worth stating that the insignificant or poor correlations of MgO with other major oxides and trace elements (Fig. 6a, c–d) provide compelling evidence for a negligible differentiation of olivine and clinopyroxene however weak relationship of Ni with MgO might be the result of minor fractionation of olivine to a certain extent (Fig. 6b). Likewise, Cr (173–369 ppm) and Ni (24.73–150.01 ppm) contents of the studied gabbros also support slight fractionation of olivine. The poor relationship between Cr and V advocates that the Chilas gabbros have not suffered varying degrees of orthopyroxene fractionation

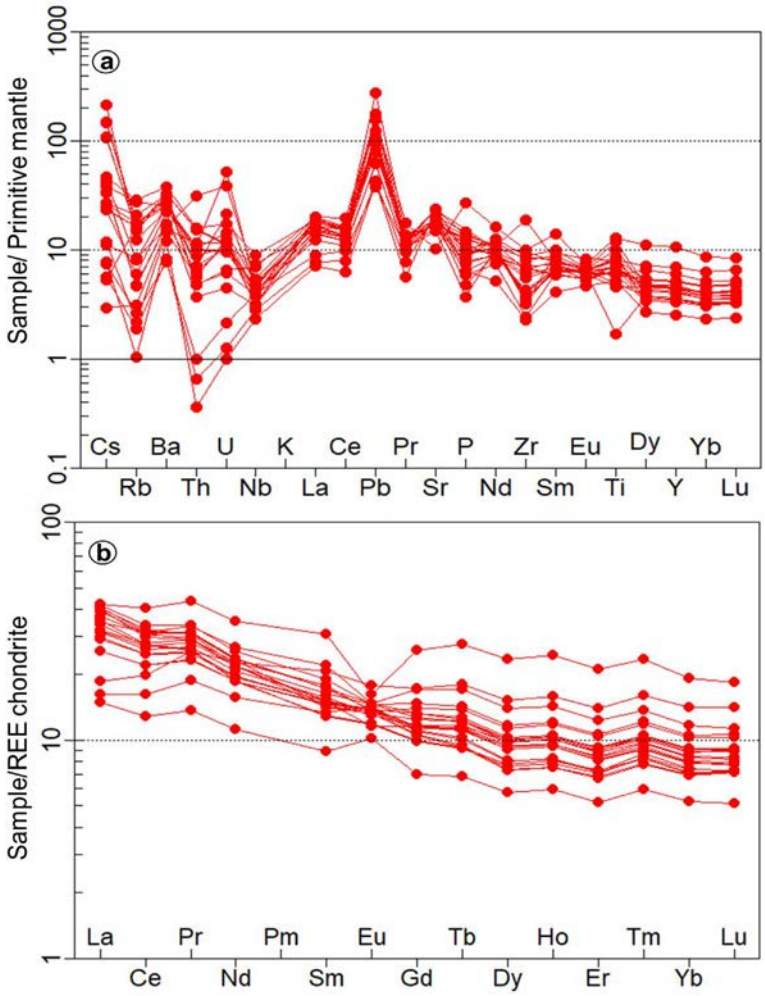

Fig. 4. Primitive mantle-normalized trace element and chondrite-normalized REE patterns of the Chilas gabbros. Primitive mantle and chondrite values are from Sun and McDonough (1989) and Nakamura (1974), respectively.

during differentiation (Fig. 6e). Similarly, Sr/Y and Eu/Eu* ratios also highlight minimal fractionation of plagioclase during its crystallization in the magma chamber (Fig. 6f; Xia et al., 2015). Likewise, poor correlation of La/Sm and Dy/Yb with SiO_2 indicates insignificant amphibole fractionation (Fig. 6g–h; Davidson et al., 2007). Based on these pieces of evidence, we assume that the Chilas gabbros reflect the characteristics of primary basaltic magma, particularly for the massive gabbroic part. However, ultramafic association (coexisting olivine, clinopyroxene, and plagioclase) in the Chilas Complex are strongly pointing towards fractionation process, hence are of cumulate origin as proposed by previous researchers (Bilqees et al., 2016; Jagoutz et al., 2006, 2007; Khan et al., 1989).

5.1.5. Fluid/Melt Metasomatism

The studied gabbros exhibit negative anomalies of HFSE (Fig. 4a), therefore, the metasomatic media were most likely fluids instead of melts. The investigated samples, when plotted on geochemical diagrams, indicate a dual-evolutionary trend, which is displayed in terms of fluid or melt-related enrichments (Fig. 7). The samples of the present study express higher values of Th/Zr, lower values of Nb/Zr, and display fluid contribution and metasomatic trend in the binary plot of Nb/Zr vs. Th/Zr (Fig. 7a; Zhong et al., 2017). However, the greater Th/Yb ratios can be attributed to the input of subducted sediments, whereas higher Sr/Nd ratios can be ascribed to the participation of slab-derived fluids (Xu et al., 2014). Gabbros of the Chilas Complex, displaying relatively higher Sr/Nd ratios (9.76–70.28, average 31.87) in comparison to the upper crust (11.85, Xu et al., 2014b) and N-MORB (12.33, Sun and McDonough, 1989), suggest that these rocks were metasomatized by fluid in the mantle wedge or a subduction system. Apart from this, geochemical plotting of Nb/Y vs. Rb/Y and Nb/Zr vs. Ce/Y (Fig. 7b–c) are in favour of fluids participation during the genesis of the gabbroic rocks.

Additionally, the movement of incompatible elements in fluids varies considerably, for instance, Th is less whereas Ba is extremely mobile (Zhong et al., 2017), and therefore fluids liberated from subducted material and their contact with mantle sources likely generate higher Ba/Th ratios in gabbros. Gabbroic samples containing lower $(La/Sm)_N$ ratios suggest a prime and significant role of fluids. The Ba/Th vs. $(La/Sm)_N$ diagram, higher Ba/Th, and lower $(La/Sm)_N$ ratios highlight that these rocks were metasomatized via fluids rather than melts (Fig. 7d; Zhong et al., 2017). The minor variation in $(La/Sm)_N$ (0.94–2.99) against a large range of Nb/U (3.03–78.57) and Nb/Th (1.47–55) exhibit the involvement of fluids that chemically metasomatized the Chilas rocks (Polat and Kerrich, 2000). Other geochemical plots, such as Ba/La vs. Th/Yb (Fig. 7e), $(Ta/La)_N$ vs. $(Hf/Sm)_N$ (Fig. 7f, Flèche et al., 1998) also illustrate the affinity of mafic rocks that are influenced by fluid-related metasomatism. Based on these findings, it is concluded that gabbros of the Chilas Complex were most likely derived from a mantle source but were modified by contributions of fluid-related metasomatism during late-stages.

5.1.6. Evaluation of alteration impacts

Low values of LOI in gabbros generally reveal a lesser impact of secondary alterations on the bulk rock geochemistry (Polat and Hofmann,

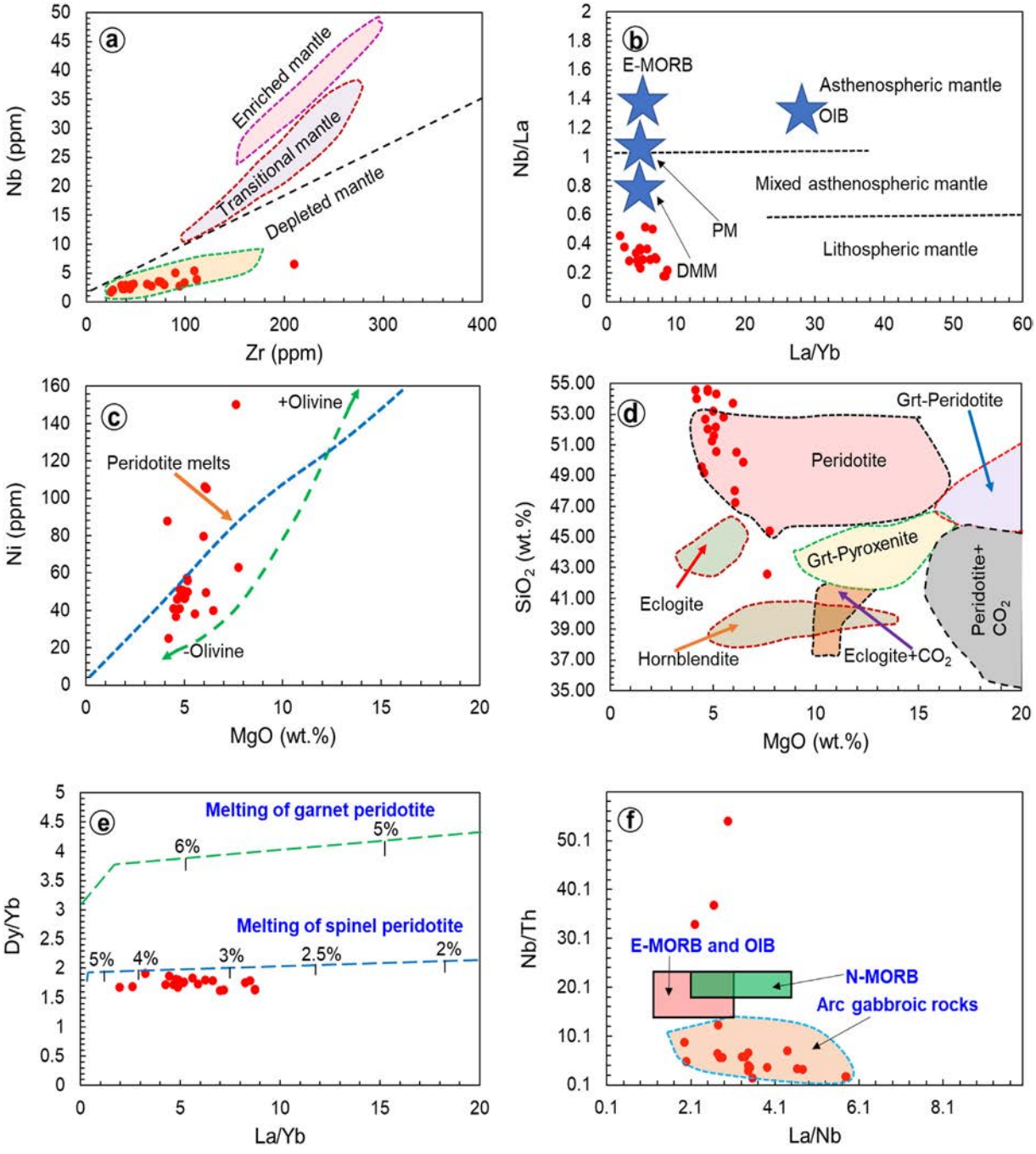

Fig. 5. Geochemical plots of the analyzed gabbros: (a) Zr vs. Nb (Geng et al., 2011); (b) La/Yb vs. Nb/La; (c) MgO vs. Ni (Herzberg, 2011); (d) MgO vs. SiO_2 (Cen et al., 2016); (e) Dy/Yb vs. La/Yb (Jung et al., 2006); (f) Nb/Th vs. La/Nb (Zhang et al., 2012).

2003). Values of LOI (0–3.24 wt%, average 1.23 wt%) and lack of Ce anomalies (Fig. 4b) in the studied samples provide credible evidence for the insignificant influence of hydrothermal alteration as proposed by Polat and Hofmann (2003). This is evidenced by the microscopic investigation also as most of the gabbroic samples have mineral assemblage with no contrasting alteration. In terms of major element compositions, mainly alkali components are prone to chemical modifications hence enrichment of these elements in gabbros can be attributed to alteration (Bischoff and Dickson, 1975). To distinguish the degree of mobility of alkali elements, studied samples from the Chilas gabbros were plotted on the $Na_2O + K_2O$ vs. Na_2O/K_2O diagram where all the samples fall in the field of unaltered gabbros (Fig. 8a), therefore proposing that the bulk chemical constituents represent the primary signatures of parental magma.

Several pieces of research on gabbros have documented that the amounts of LILEs (e.g., Rb, Sr, and Pb) can be influenced by ocean-floor metamorphism or seawater alteration (e.g., Zhong et al., 2015). On the contrary, REEs (represented by Yb and La), compatible elements (e.g., Cr and Ni) and HFSEs; (e.g., Y, Nb, Ta, Ti, and Hf), are fairly considered as immobile in low-grade metamorphism and hydrothermal alteration. Zirconium has been broadly considered as an alteration-independent index because of its immobility during hydrothermal alteration and metamorphism, hence it can be used as a significant geochemical tracer to evaluate rocks for the degree of alteration (Zhong et al., 2017). When La, Ta, Hf, and Y values were plotted against Zr (Fig. 8b–e), the interpreted samples display positive correlations between these elements and Zr, signifying

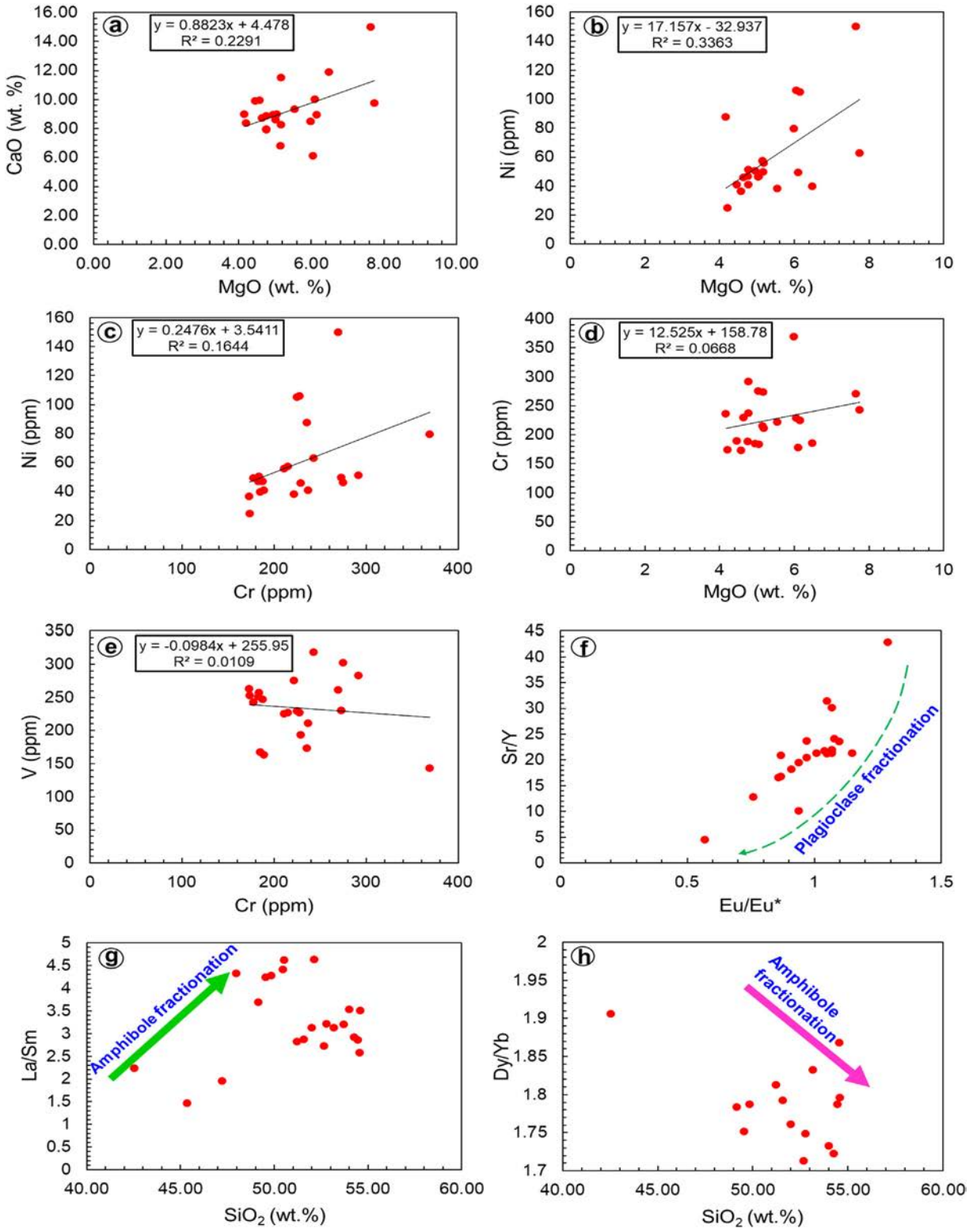

Fig. 6. Plots of selected elements, various oxides, and trace elemental ratios to trace fractional crystallization in gabbros.

that the HFSEs specifically Ta, Zr, and Hf, and REEs including La, were not influenced by hydrothermal alteration, hence reflect the signatures of primary basaltic magma. Additionally, the so-called mobile LILEs such as Rb exhibit positive correlation with Zr, also indicate minimal alteration of the samples (Fig. 8f). The Ce anomaly is commonly considered as an index for alteration with Ce/Ce* values of 0.9–1.1 as a threshold for REE immobility (Polat et al., 2002). The Chilas Complex samples indicate Ce/Ce* from 0.92 to 1.01, further confirm an insignificant impact of alteration on REE. In summary, we conclude that immobile elements (e.g., HFSEs, REEs, and LILEs) are worthwhile in considering the petrogenetic as well as for geodynamic interpretations of the gabbroic rocks.

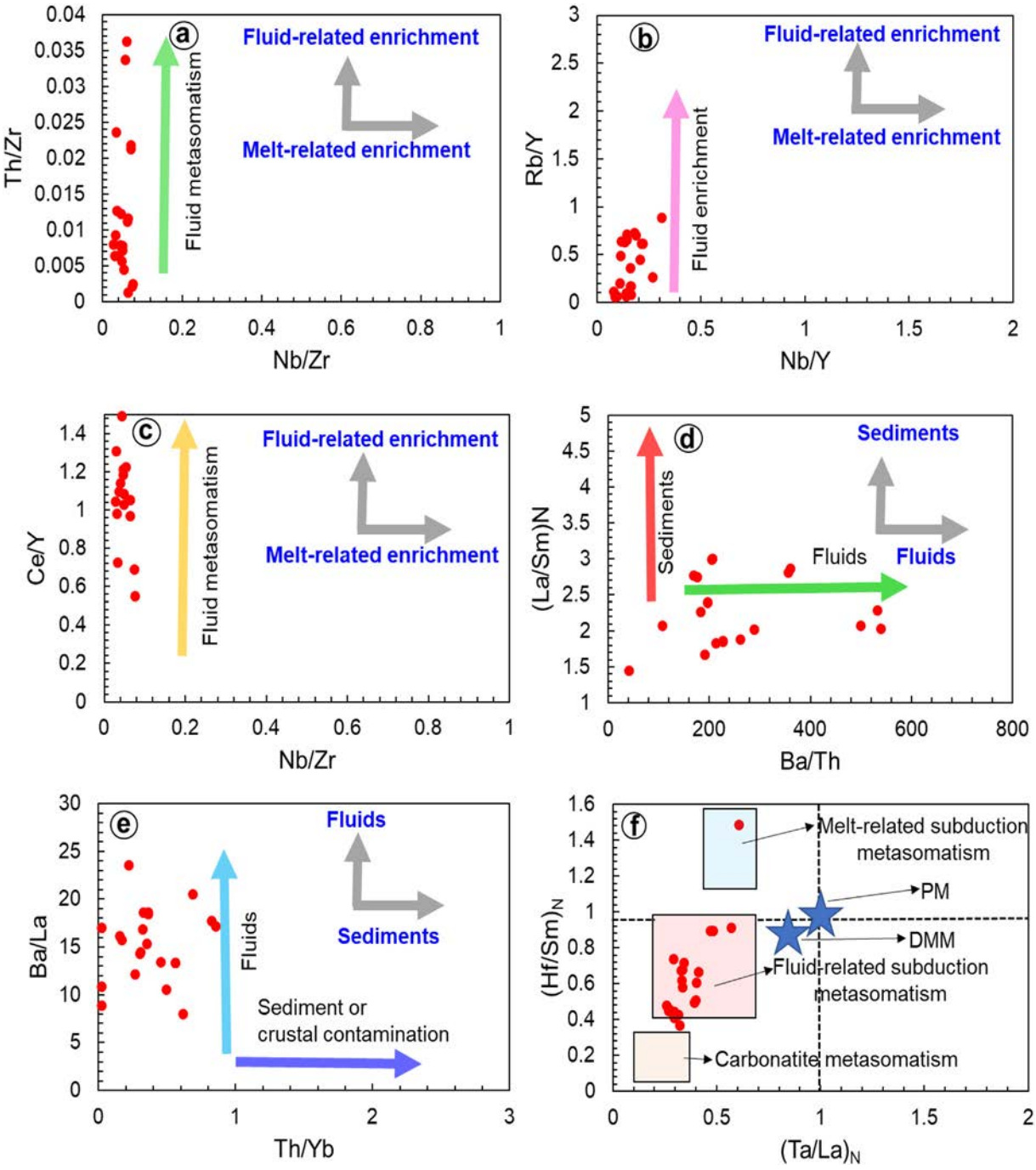

Fig. 7. Binary plots of gabbros for interpretation of fluid metasomatism in rock samples. (a) Nb/Zr vs. Th/Zr; (b) Nb/Y vs. Rb/Y; (c) Nb/Zr vs. Ce/Y; (d) Ba/Th vs. $(La/Sm)_N$; (e) Ba/La vs. Th/Yb; (f) $(Ta/La)_N$ vs. $(Hf/Sm)_N$.

5.2. Inferences from PGEs

5.2.1. Melting aspects and PGE variations

Past studies showed high melt partition co-efficient of PGEs in sulphide-silicate association and interpreted it for low-degree partial melting of magmas (Naldrett, 2010). Gabbroic rocks of lower Pd/Ir ratios with relatively higher Pt and Pd contents indicate low-degree partial melting. At low-degree partial melting, sulphides are generally retained in the residue ascribing to lower concentrations of PGEs in the silicate melt (Naldrett, 2010). Gabbros of the Chilas Complex are exhibited by lower concentrations of PGEs and the lower Pd/Ir 0.76–40.04 (exception of 77.05, 85.93 in two samples) ratios demonstrate the parental magma was likely generated by low-degree partial melting of a spinel lherzolite mantle source. Likewise, enhancement of Pt (0.63–13.75 ppb) and Pd (0.43–13.87 ppb) in Chilas samples also provide a reliable clue in favour of low-degree partial melting. At low-degree melting, sulphides were not entirely dissolved but were possibly retained in the residue. Although the majority of the samples investigated in this study show low concentrations of PGEs except for a few samples (see Table 3) that have higher concentrations of PGEs. The Pd contents (0.43–13.87 ppb) and Pd/Ir ratios (0.76–40.04, exceptions of 77.05, 85.93 for two samples) are relatively high compared to the values of Pt (0.63–13.75 ppb) and Pt/Pd (0.76–7.89) in most samples. These

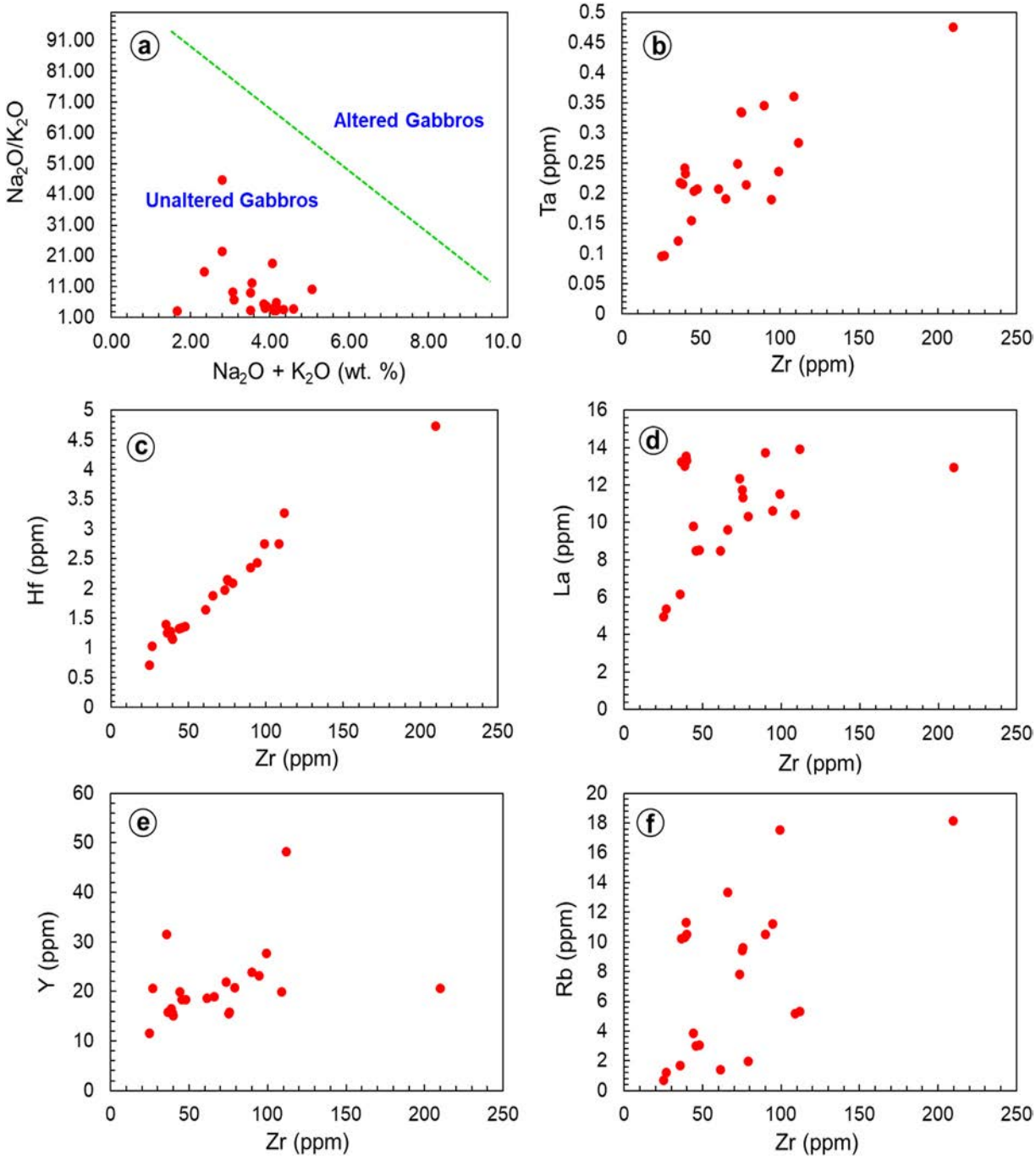

Fig. 8. (a) Plot of $Na_2O + K_2O$ vs. Na_2O/K_2O (Miyashiro, 1975) illustrating the unaltered nature of the gabbros; (b-f) Plots of Ta, Hf, La, Y and Rb vs. Zr used to assess element mobility during alteration.

features indicate an input of PGEs from the slab-dehydrated fluids and hydrous melting of depleted mantle wedge under high-fluid pressure and temperatures in subduction zones. The relative and obvious enhancement of PPGE over IPGE in some enriched samples (distinctive enrichments of Pd comparative to Pt) suggests multi-stage petrogenetic processes marked by the input of fluids, mantle metasomatism, and enhancement of incompatible elements. The higher Pd amounts in the studied samples indicate subduction influx into the mantle source. The lower Pt/Pd ratios reveal the decoupling of Pt from Pd during olivine fractional crystallization and early phases of magmatic fractionation (Said et al., 2011). The PGEs concentrations of the studied Chilas gabbros, compared with the values reported for a fertile primitive upper mantle (Os: 3.9 ± 0.5 ppb, Ru: 7.0 ± 0.9 ppb, Ir: 3.5 ± 0.4 ppb, Pd: 7.1 ± 1.3 ppb, and Pt: 7.6 ± 1.3 ppb; Becker et al., 2006) clearly indicate a depleted mantle source for their production (Table 3).

5.2.2. PGE fractionation

During initial phases of magmatic differentiation, fractional crystallization of silicates specifically olivine cause decoupling of Pt from Pd and triggers lower Pt/ Pd ratios (Said et al., 2011). Therefore, lower Pt/Pd ratios (0.76–7.89) in gabbroic rocks observed in this study can be attributed to fractional crystallization of olivine. Also, a weak relationship of Ni vs. MgO and contents of Cr (173–369 ppm) and Ni (24.73–150.01 ppm)

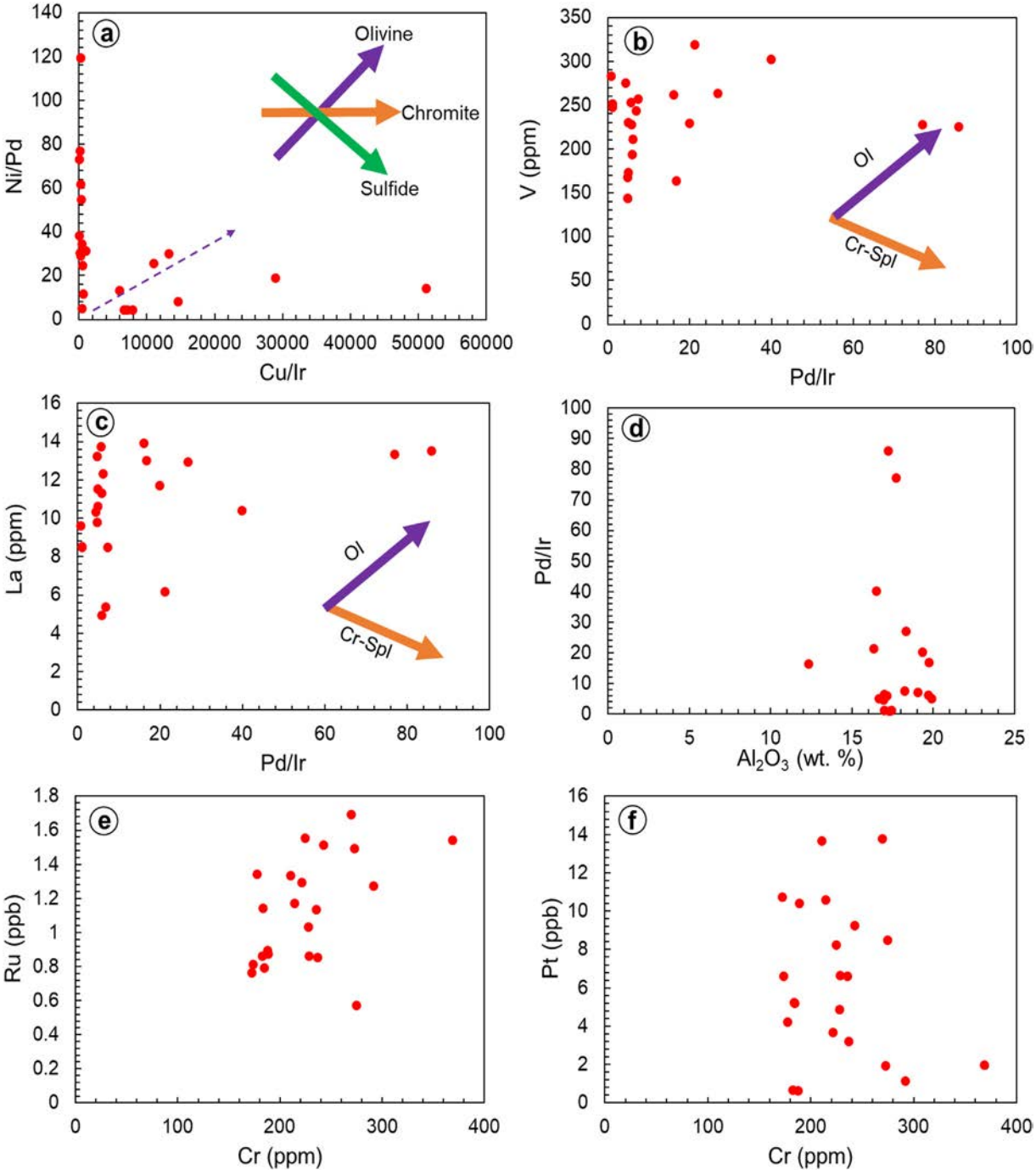

Fig. 9. (a) The variation diagram Cu/Ir vs. Ni/Pd of Chilas gabbros demonstrating olivine fractionation trend (Barnes et al., 1985); (b-c) Covariations of Pd/Ir ratios with La and V contents; (d) Plot of Al_2O_3 vs. Pd/Ir; (e-f) Plots of Cr against Ru and Pt.

supports slight fractionation of olivine (Fig. 6b). Moreover, the depletion of IPGEs comparative to PPGEs is deduced to result from initial fractionation of olivine and laurite.

Some researchers (e.g. Luguet et al., 2001) suggested Pd/Ir as an effective index of PGE fractionation during the petrological processes. An increase in the Pd/Ir ratio with increasing differentiation trends suggests magmatic fractionation whereas the ratio ca. ~1 indicates unfractionated materials. Higher Pd/Ir ratios in the Chilas gabbros can be ascribed to (1) low-degree partial melting that prompt IPGEs forming a melt depleted in IPGE, and (2) low Ru and Ir contents propose fractional crystallization of silicates such as olivine. In Cu/Ir vs. Ni/Pd diagram, the studied gabbros express prevailing trends that are consistent with the fractionation of silicate in the parental magma and attest to the distribution of platinum group elements in mafic bodies that were mainly governed by the olivine fractionation (Fig. 9a). This analytical interpretation suggests that olivine can conceivably control the PGEs distribution during magmatic evolution. Plots of V-Pd/Ir and La-Pd/Ir and covariance between Pd/Ir and V, La further indicate olivine governance on the distribution of PGEs during Chilas mafic magmatic evolution (Fig. 9b–c). It is known that Pt/Pd ratios increase by late fractionation of silicates, PGEs, chromites, and decoupling of Pt from Pd via crystal differentiation (Said et al., 2011). The measured ratios of Pt/Pd for the studied gabbros, ranging between 0.76 and 7.89, are higher than the primitive mantle values (cf. 1.82; McDonough and Sun, 1995) and can

be ascribed to fractionation of olivine. Further, the increasing Pd/Ir ratios in the studied gabbros within a limited range of Al_2O_3 (Fig. 9d), propose differential fractionation of less compatible PPGEs from IPGEs during the variable degree of melt extraction. The positive correlation of PGEs such as Ru and Pt against Cr also implies fractionation during magmatic differentiation (Mondal et al., 2019; Fig. 9e–f). The calculated Pd/Pt ratios (0.12–1.31) are significantly higher in contrast to average Pd/Pt ratios of the mantle (0.57; Taylor and McLennan, 1985) attesting to PGEs depletion in the parental magma.

5.2.3. Possible causes for PGEs depletions

One promising clarification for PGEs depletions in gabbros is considered as prior sulphide segregation. It is reported that the extreme decline of PGEs can be generated by sulphide segregation (Song et al., 2009). Early sulphide segregation from silicate magma may cause additional depletion of PGEs in the magma because PGEs indicate higher partition coefficients between sulphide and silicate melt in contrast to the base metals. Cu/Zr ratio is a sensitive pointer of sulphide segregation because both Zr and Cu have opposite characters during sulphide

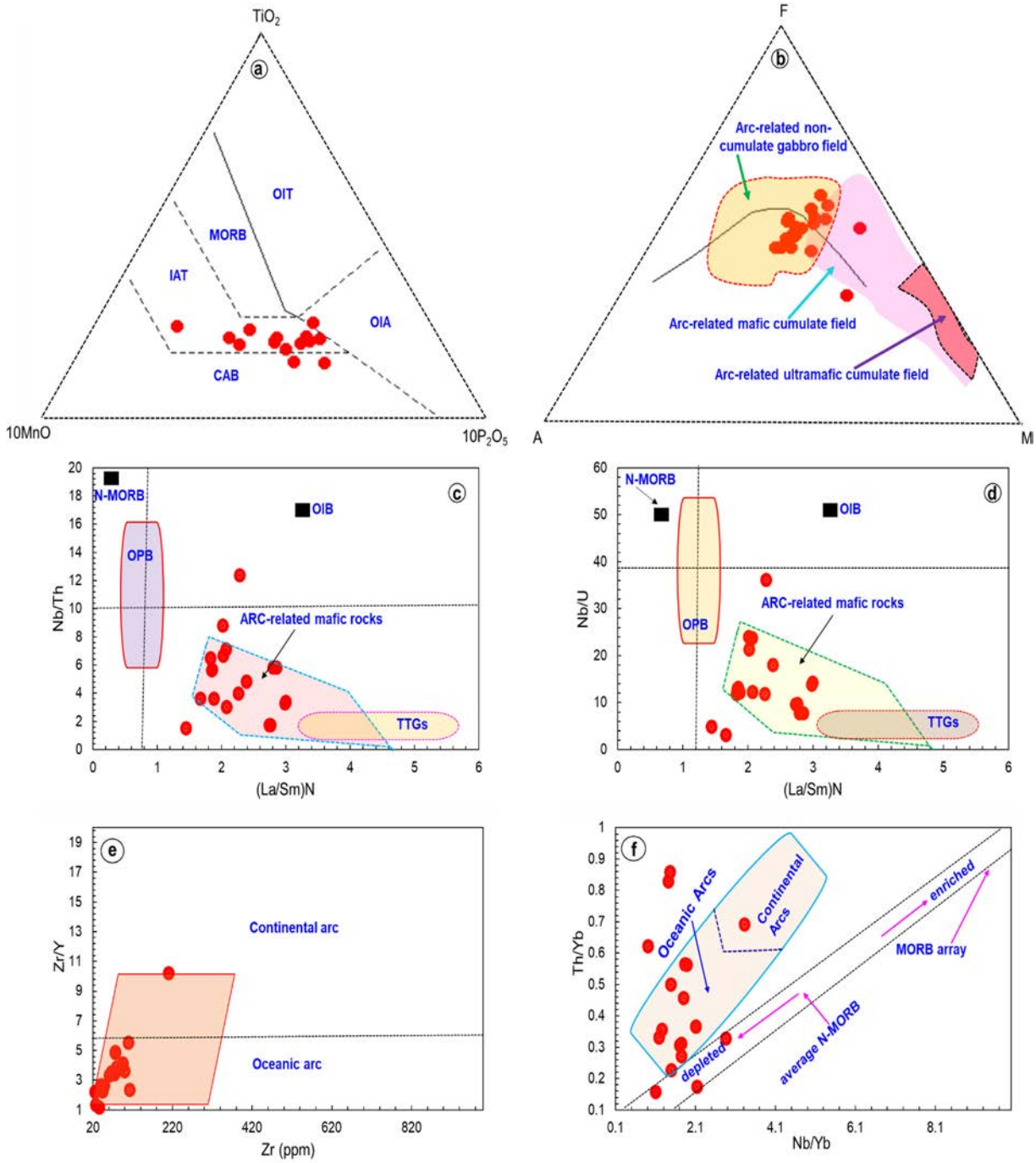

Fig. 10. Geochemical diagrams for tectonic settings of the Chilas gabbros: (a) MnO-TiO_2-P_2O_5 (Mullen, 1983); (b) A ($Na_2O + K_2O$), F (FeO^T), M (MgO) (Irvine and Baragar, 1971). Fields of cumulate and non-cumulate natures are after Beard (1986); (c-d) $(La/Sm)_N$ vs. Nb/Th and $(La/Sm)_N$ vs. Nb/U; (e) Zr/Y vs. Zr (Pearce, 1983); (f) Th/Yb vs. Nb/Yb (Pearce and Peate, 1995). Abbreviations: ARC = arc-related basalts; CAB = Calc-Alkaline Basalt; IAT = Island Arc Tholeiite; MORB = Mid Oceanic Ridge Basalt; N-MORB = Normal Mid-Ocean Ridge Basalt; OIA = Ocean Island Alkaline Basalt; OIB = Oceanic Island Basalts; OPB = Oceanic Plateau Basalts; OIT = Ocean Island Tholeiite; TTGs = Tonalite–Trondhjemite–Granodiorites. Lines of OIB, MORB, and primitive mantle-normalizing values are from Sun and McDonough (1989). Shaded areas of OPB and TTGs are adapted from Polat and Kerrich (2000).

separation. The gabbros of Chilas Complex, having Cu/Zr ratios higher than 1 (Table 2), suggest a lack of sulphide separation preceding emplacement (Wang et al., 2006). Meanwhile, Cu/Pd ratio, another useful proxy to evaluate sulphide segregation in mafic rocks, considerably lower in Chilas gabbros (11.55 to 3161.29) compared with the primitive mantle value (Cu/Pd = 7000; Barnes and Maier, 1999), thereby demonstrating lack of sulphide segregation during magmatic evolution. All these pieces of evidence suggest that the mafic rocks had insignificant sulfide separation prior to their emplacement, therefore sulphide segregation cannot be a promising cause for PGEs depletion. The PGE depletions in the parental magma of the Chilas gabbros are most likely sulfide retention in the mantle source owing to low-degree partial melting or from a PGE-depleted mantle source (Song et al., 2016).

5.2.4. Sulphide saturation

According to Naldrett (2010), PGE abundances in mafic bodies differ in the sequence of increasing compatibility (Ir < Ru < Pt < Au < Pd) under sulphur undersaturated conditions. In this study, the same sequence of increasing compatibility can be observed (see Table 3), suggesting S-undersaturation in Chilas gabbros.

During magmatic differentiation S and Cu behave similarly hence Cu can be used as a proxy for sulphur. Meanwhile, Pd being the most chalcophile among all PGEs, and its abundance is governed through S-saturation and precipitation from a melt. Therefore, both Cu and Pd have been documented as a worthwhile pointer of the degree of S-saturation of magmas (Chen and Xia, 2008). The Chilas mafic rocks exhibit Cu/Pd ratios (11–3161) considerably lower in comparison to primitive mantle value (Cu/Pd = 7000; Barnes and Maier, 1999), thereby confirming S-undersaturated parental magma. Trace element and PGEs contents of the gabbros, noticed by Ni = 24.7–87.5 ppm (exception of 105 and 150 ppm), ∑PGE = 2.77–30.47 ppb and ∑PPGE = 1.33–28.98 ppb, advocate sulphide unsaturation and PGE depletion. Meanwhile, the positive correlation of PGEs such as Ru and Pt against Cr further implies the S-undersaturated role of the magma (Mondal et al., 2019; Fig. 9e–f). Likewise, Os diminution in these rocks reflects Os fractionation through mantle processes involving sulphides dissolution resulting in S-undersaturation, thus verifying and supporting S-undersaturation in the parental magma. These findings are consistent with the PGEs interpretations of mafic flows reported from the Belingwe greenstone belt, Zimbabwe (Zhou, 1994). In summary, the Cu/Pd ratios of gabbroic rocks (Cu/Pd = 11–3161) in combination with the dominancy of Pd (0.43 ppb–13.87 ppb) over Pt (0.63 ppb–13.75 ppb) can be ascribed to the influx of subduction-derived fluids into the mantle wedge and production of magma under S-undersaturated conditions. The S-undersaturation in Chilas gabbros with relatively low Ti and Fe concentrations indicates the generation of its parental magma at a shallow level in the subduction zone setting.

6. Geodynamic implications

Tholeiitic/mafic rocks are generally formed under various tectonic settings, such as Mid-ocean ridge, Intra-continent, Ocean island, Back-arc basin, and Island arc. Hence, numerous discrimination diagrams can be constructed to distinguish the tectonic environments in which the rocks form. In the MnO-TiO_2-P_2O_5 triangular tectonic discrimination diagram (Fig. 10a), the Chilas gabbros fall in the field of island arc tholeiite (IAT) supporting for the arc magmatism. On the AFM triangular plot (Fig. 10b), the Chilas rocks plot in the arc-related mafic-non cumulate fields, again, suggesting an affinity for arc magmatism. Further, the binary diagrams of Nb/Th, Nb/U vs. $(La/Sm)_N$ also indicate arc setting for the Chilas gabbros (Fig. 10c–d). Moreover, the data also plot in the oceanic field and arc-tholeiite domain in the Zr–Zr/Y and Nb/Yb vs. Th/Yb tectonic diagrams, confirming oceanic arc affinity for the gabbroic rocks of the Chilas Complex (Fig. 10e–f).

Low contents of Rb (0.65–18.10 ppm), Nb (1.65–6.46 ppm), and Y (11.50–48.13 ppm) as pointed out by Pearce et al. (1984) enhance our interpretation for the arc environment. Likewise, negative anomalies of Nb, Zr, and Ti combined with higher contents of LILEs and LREEs (Pearce et al., 1984; Ugarkar, 2017, and references therein) in the Chilas gabbros suggest arc magmatism in convergent settings (Fig. 4). Considering the above aspects, we conclude that the geochemical data of Chilas gabbros provide credible evidence in favour of arc magmatism in oceanic island arc tectonic affinity and is comparable with the arc-related Alaskan-type mafic magmatism (Abdallah et al., 2019).

Trace element spider diagrams and comparable oceanic island arc tectonic affinity of the Chilas Complex highlight its origin that can be linked with oceanic island arc setting in the Neo-Tethys Ocean during the Early to Mid-Cretaceous. Keeping in view these grounds, it is plausible to propose that the Chilas Complex represent a fragment of the oceanic island arc system.

Based on geological and geochemical interpretations, we present a plausible tectonic model that defines the tectonic and magmatic processes involved in the evolution of gabbroic rocks of the Chilas Complex (Fig. 11). The convergent settings of the KIA (including the Chilas Complex) are manifested by the northward subduction of the Indian plate beneath the Eurasian plate. The subducted lithosphere led to the activation of arc magmatism within the Neo-Tethys Ocean. The subduction continuation of the descending oceanic crust of the Indian plate and its dehydration would likely provide a dense medium in the downgoing slab that would have endorsed the rise of the lithospheric mantle,

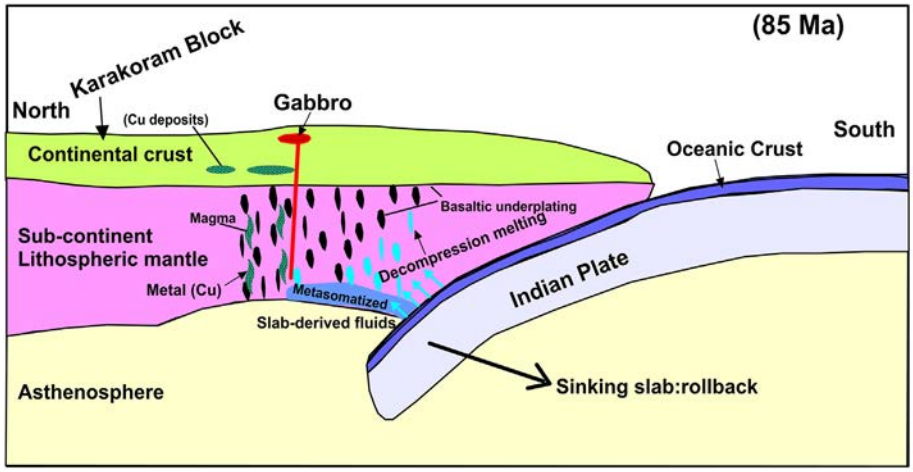

Fig. 11. Schematic model indicating the petrogenesis and tectonic evolution of Cretaceous (85 Ma) gabbros from the Chilas Complex.

implying the generation of mafic magmas in the sub-continental lithospheric mantle wedge. The mafic magma was likely derived from a spinel-bearing mantle source, forming the Chilas gabbros under partial-melting conditions, and was further metasomatized by the slab-derived fluids at shallow depth. The fluid-transfer from subducted slab to mantle wedge may result in flux and decompression melting. The significant higher ratios of Ba/Th (41.66–2786) and Ba/La (7.91–23.51) for Chilas gabbros corroborate that the decompression melting might be induced via flux of slab-derived fluids. Moreover, samples of the Chilas gabbros provide limited signatures of crustal contamination during their emplacement in an arc environment. It is worth mentioning that the mantle rise generating the Chilas mafic complex can be considered as a significant event in the crustal evolutionary history of the Kohistan arc. This important event possibly delivered the requisite heat and magma to produce gigantic batholith of Kohistan granitoids. A similar geodynamic scenario can be compared with recently stated geodynamic settings of mafic rocks of the Sonakhan Greenstone Belt of Bastar Craton, Central India (Manu Prasanth et al., 2017).

7. Conclusions

1) The magma source of the Chilas Complex gabbros was derived from a depleted mantle source. The gabbros were produced in spinel stability and reflect the characteristics of primary basaltic magma with the negligible role of fractional crystallization.
2) The presence of water-rich minerals (hornblende) and higher Al/Ti ratios of clinopyroxene suggest that the parental magma was wet. The studied rocks were metasomatized by fluid-enriched source and hydrothermal alteration was insignificant that could chemically modify the gabbros.
3) PGEs data indicate the generation of these rocks through low-degree partial melting of their parental magma. Moreover, slab-dehydrated fluids played a significant role to metasomatize the mantle. The lower values of PGEs in the studied gabbros indicate a depleted mantle source.
4) Sulphur-undersaturation in the studied gabbros along with low Ti and Fe indicate magma generation at the shallow level from a spinel-bearing peridotite mantle source.
5) Tectonically the Chilas gabbros were likely formed from a lithospheric mantle source that was partially metasomatized by slab derived fluids in the mantle wedge in subduction-related arc environment.

Declaration of Competing Interest

None.

Acknowledgements

We are thankful to the Institute of Geochemistry, Chinese Academy of Science, China, for their assistance in laboratory work. We highly appreciate critical comments by the editor and two anonymous reviewers which significantly improved the earlier version of the manuscript. This work was funded by the Special Fund of the State Key Laboratory of Ore Deposit Geochemistry, the Special Fund for the construction of "Double First-Class" disciplines in Jiangxi Province (2400100017) and the Jiangxi "Double Thousand Plan".

References

Abdallah, S.E., Ali, S., Obeid, M.A., 2019. Geochemistry of an Alaskan-type mafic-ultramafic complex in Eastern Desert, Egypt: New insights and constraints on the Neoproterozoic island arc magmatism. Geosci. Front. 10, 941–955.

Ali, A., Nakamura, E., Yamamoto, H., 2002. Sm–Nd mineral ages of pegmatite veins and their host rocks from Swat area, Chilas complex, northern Pakistan. J. Asian Earth Sci. 21, 331–339.

Bard, J.P., 1983. Metamorphism of an obducted island arc: example of the Kohistan sequence (Pakistan) in the Himalayan collided range. Earth Planet. Sci. Lett. 65, 133–144.

Barnes, S.J., Maier, W.D., 1999. The fractionation of Ni, Cu and the noble metals in silicate and sulphide liquids. Short Course Notes-Geological Association of Canada 13, 69–106.

Barnes, S.J., Naldrett, A.J., Gorton, M.P., 1985. The origin of the fractionation of platinum-group elements in terrestrial magmas. Chem. Geol. 53, 303–323.

Beard, J.S., 1986. Characteristic mineralogy of arc-related cumulate gabbros: Implications for the tectonic setting of gabbroic plutons and for andesite genesis. Geology 14, 848–851.

Becker, H., Horan, M.F., Walker, R.J., Gao, S., Lorand, J.P., Rudnick, R.L., 2006. Highly siderophile element composition of the Earth's primitive upper mantle: constraints from new data on peridotite massifs and xenoliths. Geochim. Cosmochim. Acta 70, 4528–4550.

Bilqees, R., Jan, M.Q., Khan, M.A., Windley, B.F., 2016. Silicate-oxide mineral chemistry of mafic-ultramafic rocks as an indicator of the roots of an island arc: The Chilas Complex, Kohistan (Pakistan). Island Arc 25, 4–27.

Bischoff, J.L., Dickson, F.W., 1975. Seawater-basalt interaction at 200 °C and 500 bars: implications for origin of sea-floor heavy-metal deposits and regulation of seawater chemistry. Earth Planet. Sci. Lett. 25, 385–397.

Brunelli, D., Cipriani, A., Bonatti, E., 2018. Thermal effects of pyroxenites on mantle melting below mid-ocean ridges. Nat. Geosci. 11, 520–525.

Burg, J.P., Bodinier, J.L., Chaudhry, S., Hussain, S., Dawood, H., 1998. Infra-arc mantle-crust transition and intra-arc mantle diapirs in the Kohistan Complex (Pakistani Himalaya): petro-structural evidence. Terra Nova-Oxford 10, 74–80.

Cen, T., Li, W.X., Wang, X.C., Pang, C.J., Li, Z.X., Xing, G.F., Zhao, X.L., Tao, J., 2016. Petrogenesis of early Jurassic basalts in southern Jiangxi Province, South China: Implications for the thermal state of the Mesozoic mantle beneath South China. Lithos 256, 311–330.

Chen, G., Xia, B., 2008. Platinum-group elemental geochemistry of mafic and ultramafic rocks from the Xigaze ophiolite, southern Tibet. J. Asian Earth Sci. 32, 406–422.

Condie, K., 2015. Changing tectonic settings through time: indiscriminate use of geochemical discriminant diagrams. Precambrian Res. 266, 587–591.

Cox, K.G., Bell, J.D., Pankhurst, R.J., 1979. The Interpretation of Igneous Rocks. George Allen and Unwin, London, p. 450.

Davidson, J., Turner, S., Handley, H., MacPherson, C., Dosseto, A., 2007. Amphibole "sponge" in arc crust? Geology 35, 787.

Dhuime, B., Bosch, D., Bodinier, J.-L., et al., 2007. Multistage evolution of the Jijal ultramafic-mafic complex (Kohistan, N Pakistan): Implications for building the roots of island arcs. Earth Planet. Sci. Lett. 261, 179–200.

Falloon, T.J., Green, D.H., Danyushevsky, L.V., Mcneill, A.W., 2008. The composition of near-solidus partial melts of fertile peridotite at 1 and 1.5 GPa: implications for the petrogenesis of MORB. J. Petrol. 49, 591–613.

Flèche, M.R.L., Camiré, G., Jenner, G.A., 1998. Geochemistry of post-Acadian, Carboniferous continental intraplate basalts from the Maritimes Basin, Magdalen Islands, Québec Canada. Chem. Geol. 148, 115–136.

Gaetani, G.A., Grove, T.L., 1998. The influence of water on melting of mantle peridotite: Contrib. Mineral. Petrol. 131, 323–346.

Geng, H., Sun, M., Yuan, C., Zhao, G., Xiao, W., 2011. Geochemical and geochronological study of early Carboniferous volcanic rocks from the West Junggar: Petrogenesis and tectonic implications. J. Asian Earth Sci. 42, 854–866.

George, M.T., Harris, N.B.W., Butler, R.W.H., 1993. The tectonic implications of contrasting postcollisional magmatism between the Kohistan island arc and the Nanga Parbat-Haramosh massif, Pakistan Himalaya. In: Searle, M.P., Treloar, P.J. (Eds.), Himalayan Tectonics. Geological Society of London Special Publication vol. 74, pp. 173–191.

Herzberg, C., 2011. Identification of source lithology in the Hawaiian and Canary Islands: implications for origins. J. Petrol. 52, 113–146.

Irvine, T.N., Baragar, W.R.A., 1971. A guide to the chemical classification of the common volcanic rocks. Can. J. Earth Sci. 8, 523–548.

Jagoutz, O., 2014. Arc crustal differentiation mechanisms. Earth Planet. Sci. Lett. 396, 267–277.

Jagoutz, O., Müntener, O., Burg, J.P., Ulmer, P., Jagoutz, E., 2006. Lower continental crust formation through focused flow in km-scale melt conduits: the zoned ultramafic bodies of the Chilas Complex in the Kohistan Island arc (NW Pakistan). Earth Planet. Sci. Lett. 242, 320–342.

Jagoutz, O., Müntener, O., Ulmer, P., Pettke, T., Burg, J.P., Dawood, H., Hussain, S., 2007. Petrology and mineral chemistry of lower crustal intrusions: The Chilas Complex, Kohistan (NW Pakistan). J. Petrol. 48, 1895–1953.

Jung, C., Jung, S., Hoffer, E., Berndt, J., 2006. Petrogenesis of Tertiary mafic alkaline magmas in the Hocheifel, Germany. J. Petrol. 47, 1637–1671.

Khan, M.A., Jan, M.Q., Windley, B.F., Tarney, J., Thirlwall, M.F., 1989. The Chilas mafic–ultramafic igneous complex; the root of the Kohistan Island Arc in the Himalaya of northern Pakistan. Geol. Soc. Am. 232, 75–94.

Khan, M.A., Jan, M.Q., Weaver, B.L., 1993. Evolution of the lower arc crust in Kohistan, N. Pakistan: Temporal arc magmatism through early, mature and intra-arc rift stages. In: Treloar, P.J., Searle, M.P. (Eds.), Himalayan Tectonics. Geological Society of London Special Publication vol. 74, pp. 123–138.

Khan, S.D., Walker, D.J., Hall, S.A., Burke, K.C., Shah, M.T., Stockli, L., 2009. Did the Kohistan-Ladakh island arc collide first with India? Geol. Soc. Am. Bull. 121, 366–384.

Kubo, K., Sawada, Y., Takahashi, Y., Kausar, A.B., Seki, Y., Khan, I.H., Khan, T., Khan, N.A., Takahashi, Y., 1996. The Chilas Igneous Complex in the Western Himalayas of Northern Pakistan. Proceedings of Geoscience Colloquium, Geoscience Laboratory, Geological Survey of Pakistan, Islamabad 15, 63–68.

Loucks, R.R., 1990. Discrimination of ophiolitic from non ophiolitic ultramafic-mafic allochthons in orogenic belts by the Al/Ti ratio in clinopyroxene. Geology 18, 346–349.
Luguet, A., Alard, O., Lorand, J.P., Pearson, N.J., Ryan, C., O'Reilly, S.Y., 2001. Laser ablation microprobe (LAM)-ICPMS unravels the highly siderophile element geochemistry of the oceanic mantle. Earth Planet. Sci. Lett. 189, 285–294.
Manu Prasanth, M.P., Hari, K.R., Chalapathi Rao, N.V., Hou, G., Pandit, D., 2017. An island-arc tectonic setting for the Neoarchean Sonakhan Greenstone Belt, Bastar Craton, Central India: Insights from the chromite mineral chemistry and geochemistry of the siliceous high-Mg basalts (SHMB). Geol. J. 1–17.
McDonough, W.F., Sun, S.S., 1995. The composition of the earth. Chem. Geol. 120, 223–253.
McInnes, B.I.A., Gregoire, M., Binns, R.A., Herzig, P.M., Hannington, M.D., 2001. Hydrous metasomatism of oceanic sub-arc mantle, Lihir, Papua New Guinea: Petrology and geochemistry of fluid-metasomatised mantle wedge xenoliths: Earth Planet. Sci. Lett. 188, 169–183.
McKenzie, D., Bickle, M.J., 1988. The volume and composition of melt generated by extension of the lithosphere: J. Petrol. 29, 625–679.
Middlemost, E.A.K., 1985. Magmas and Magmatic Rocks. Longman, London.
Miyashiro, A., 1974. Volcanic rock series in island arcs and active continental margins. Am. J. Sci. 274, 321–355.
Miyashiro, A., 1975. Classification, characteristics, and origin of ophiolites. J. Geol. 83, 249–281.
Mondal, S.K., Khatun, S., Prichard, H.M., Satyanarayanan, M., Kumar, G.R.R., 2019. Platinum-group element geochemistry of boninite-derived Mesoarchean chromitites and ultramafic-mafic cumulate rocks from the Sukinda Massif (Orissa, India). Ore Geol. Rev. 104, 722–744.
Mullen, E.D., 1983. MnO-TiO_2-P_2O_5: a minor element discriminant for basaltic rocks of Oceanic environments and its implications for petrogenesis. Earth Planet. Sci. Lett. 62, 53–62.
Nakamura, N., 1974. Determination of REE, Ba, Fe, Mg, Na, and K in carbonaceous and ordinary chondrites. Geochim. Cosmochim. Acta 38, 757–775.
Naldrett, A.J., 2010. Secular variation of magmatic sulfide deposits and their source magmas. Econ. Geol. 105, 669–688.
Pearce, J.A., 1983. Role of sub-continental lithosphere in magma genesis at active continental margins. In: Hawkesworth, C.J., Nurry, M.J. (Eds.), Continental Basalts and Mantle Xenoliths. Shiva Publishing, Nantwich, pp. 230–249.
Pearce, J.A., Peate, D.W., 1995. Tectonic implications of the composition of volcanic ARC magmas. Annu. Rev. Earth Planet. Sci. 23, 251–285.
Pearce, J.A., Harris, N.B.W., Tindle, A.G., 1984. Trace element discrimination diagrams for the tectonic interpretation of granitic rocks. J. Petrol. 25, 956–983.
Polat, A., Hofmann, A.W., 2003. Alteration and geochemical patterns in the 3.7–3.8 Ga Isua greenstone belt, West Greenland. Precambrian Res. 126, 197–218.
Polat, A., Kerrich, R., 2000. Archaean greenstone belt magmatism and the continental growth-mantle evolution connection: Constraints from Th–U–Nb–LREE systematics of the 2.7 Ga Wawa subprovince, Superior province, Canada. Earth Planet. Sci. Lett. 175, 41–54.
Polat, A., Hofmann, A.W., Rosing, M.T., 2002. Boninite-like volcanic rocks in the 3.7–3.8 Ga Isua greenstone belt, West Greenland: geochemical evidence for intra-oceanic subduction zone processes in the early Earth. Chem. Geol. 184, 231–254.
Pudsey, C.J., 1986. The Northern Suture, Pakistan: margin of a Cretaceous island arc. Geol. Mag. 123, 405–423.
Rehman, H.U., Seno, T., Yamamoto, H., Khan, T., 2011. Timing of collision of the Kohistan–Ladakh Arc with India and Asia: debate. Island Arc 20, 308–328.
Qi, L., Hu, J., Gregoire, D.C., 2000. Determination of trace elements in granites by inductively coupled plasma mass spectrometry. Talanta 51, 507–513.
Said, N., Kerrich, R., Maier, W.D., McCuaig, C., 2011. Behaviour of Ni–PGE–Au–Cu in mafic–ultramafic volcanic suites of the 2.7 Ga Kambalda Sequence, Kalgoorlie Terrane, Yilgarn Craton. Geochim. Cosmochim. Acta 75, 2882–2910.
Saunders, A.D., Storey, M., Kent, R.W., Norry, M.J., 1992. Consequences of plume-lithosphere interactions. Geol. Soc. London Spec. Publ. 68, 41–60.
Schaltegger, U., Zeilinger, G., Frank, M., Burg, J.P., 2002. Multiple mantle sources during island arc magmatism: U-Pb and Hf isotopic evidence from the Kohistan arc complex, Pakistan. Terra Nova 14, 461–468.
Shand, 1943. Eruptive Rocks. John Wiley & Sons.
Sisson, T.W., Grove, T.L., 1993. Experimental investigations of the role of Hf-O in calc-alkaline differentiation and subduction zone magmatism: Contrib. Miner. Petrol. 113, 143–166.
Song, X.Y., Hu, R.Z., Chen, L.M., 2009. Geochemical natures of copper, nickel and PGE and their significance for the study of origin and evolution of mantle-derived magmas and magmatic sulfide deposits. Earth Sci. Front. 16, 287–305 (in Chinese with English Abstract).
Song, X.Y., Yi, J.N., Chen, L.M., She, Y.W., Liu, C.Z., Dang, X.Y., Yang, Q.A., Wu, S.K., 2016. The Giant Xiarihamu Ni-Co Sulfide Deposit in the East Kunlun Orogenic Belt, Northern Tibet Plateau. China. Econ. Geol. 111, 29–55.
Sun, S.S., McDonough, W.F., 1989. Chemical and isotopic systematics of Oceanic basalts: Implications for mantle composition and processes. In: Saunders, A.D., Norry, M.J. (Eds.), Magmatism in the Ocean Basins. Geol. Soc. London Spec. Publ vol. 42, pp. 313–345.
Takahashi, Y., Mikoshiba, M.U., Takahashi, Y., Kausar, A.B., Khan, T., Kubo, K., 2007. Geochemical modelling of the Chilas Complex in the Kohistan Terrane, northern Pakistan. J. Asian Earth Sci. 29, 336–349.
Taylor, S.R., McLennan, S.M., 1985. The Continental Crust: Its Composition and Evolution. Blackwell, Oxford, p. 312.
Treloar, P.J., Brodie, K.H., Coward, M.P., Jan, M.Q., Khan, M.A., Knipe, R.J., Rex, D.C., Williams, M.P., 1990. The evolution of the Kamila Shear Zone, Kohistan, Pakistan. In: Salisbury, M.H., Fountain, D.M. (Eds.), Exposed cross-section of the continental crust. Kluwer Academic Publishers, pp. 175–214 NATO ASI Series, C317.
Ugarkar, A.G., 2017. Geochemistry of mafic-ultramafic magmatism in the Western Ghats belt (Kudremukh greenstone belt), western Dharwar Craton, India: implications for mantle sources and geodynamic setting. Int. Geol. Rev. 59, 1507–1531.
Wang, C.Y., Zhou, M.F., Keays, R.R., 2006. Geochemical constraints on the origin of the Permian Baimazhai mafic-ultramafic intrusion, SW China. Contrib. Miner. Petrol. 152, 309–321.
Wang, Y.F., Zeng, L., Gao, J., Zhao, L., Gao, L.E., Shang, Z., 2019. Along-arc variations in isotope and trace element compositions of Paleogene gabbroic rocks in the Gangdese batholith, southern Tibet. Lithos 324, 877–892.
Williams, Q., Hemley, R.J., 2001. Hydrogen in the deep Earth: Annu. Rev. Earth Planet. Sci. 29, 365–418.
Xia, Y., Xu, X., Zhao, G., Liu, L., 2015. Neoproterozoic active continental margin of the Cathaysia block: evidence from geochronology, geochemistry, and Nd–Hf isotopes of igneous complexes. Precambrian Res. 269, 195–216.
Xu, J.F., Castillo, P.R., Chen, F.R., Niu, H.C., Yu, X.Y., Zhen, Z.P., 2003. Geochemistry of late Paleozoic mafic igneous rocks from the Kuerti area, Xinjiang, Northwest China: Implications for back-arc mantle evolution. Chem. Geol. 193, 137–154.
Xu, Y.G., Ma, J.L., Frey, F.A., Feigenson, M.D., Liu, J.F., 2005. Role of lithosphere asthenosphere interaction in the genesis of Quaternary alkali and tholeiitic basalts from Datong, western North China Craton. Chem. Geol. 224, 247–271.
Xu, M.J., Li, C., Xu, W., Xie, C., Hu, P., Wang, M., 2014. Petrology, geochemistry and geochronology of gabbros from the Zhongcang ophiolitic mélange, Central Tibet : Implications for an intra-oceanic subduction zone within the Neo-Tethys Ocean. J. Earth Sci. 25, 224–240.
Zhang, A.M., Wang, Y.J., Fan, W.M., Zhang, Y.Z., Yang, J., 2012. Earliest Neoproterozoic (ca.1.0 Ga) arc–back-arc basin nature along the northern Yunkai Domain of the Cathaysia Block: geochronological and geochemical evidence from the metabasite. Precambrian Res. 220, 217–233.
Zhong, Y., Xia, B., Liu, W.L., Yin, Z.X., Hu, X.C., Huang, W., 2015. Geochronology, petrogenesis and tectonic implications of the Jurassic Namco–Renco ophiolites. Tibet. Int. Geol. Rev. 57, 508–528.
Zhong, Y., Liu, W.L., Xia, B., Liu, J.N., Guan, Y., Yin, Z.X., Huang, Q.T., 2017. Geochemistry and geochronology of the Mesozoic Lanong ophiolitic mélange, northern Tibet: Implications for petrogenesis and tectonic evolution. Lithos 292, 111–131.
Zhou, M.F., 1994. PGE distribution in 2.7 Ga layered komatiite flows from the Belingwe greenstone belt, Zimbabwe. Chem. Geol. 118, 155–172.